Transportation Sector: Global Road Emissions

Tomek Kott[1,2], Kevin Foster[1,2], Marisel Villafane-Delgado[1,2], Wayne Loschen[1,2], Patrick Sicurello[1,2], Melat Ghebreselassie[1,2], Elizabeth Reilly[1,2] and Marisa Hughes[1,2]

1) The Johns Hopkins University Applied Physics Laboratory (JHU/APL)
2) The Climate TRACE Coalition

1 Introduction

Transportation contributed 27% of anthropogenic greenhouse gas (GHG) emissions in the United States of America (USA) for 2020, higher than any other sector, and 12.6% of all global GHG emissions in 2019 (US EPA 2023; World Resources Institute 2022). The primary source of transportation sector emissions are on-road vehicles, accounting for approximately 74% of global transportation emissions in 2018 (International Energy Agency 2019). Quantifying the distribution of on-road transportation emissions and creating timely emissions inventories are vital to identify trends, track mitigation efforts, and inform policy decisions.

Previous efforts have developed detailed bottom-up on-road emission inventories for the USA (Gately, Hutyra, and Wing 2019; Gurney et al. 2020), but do not easily extend globally due to the reliance on vehicle traffic and road data that is not always readily available. The Emissions Database for Global Atmospheric Research (EDGAR) provides a global inventory for transportation that uses road density as a proxy to spatially distribute emissions (Crippa et al. 2020). However, some emission estimates for urban centers in EDGAR deviated from other bottom-up inventories by 500%, indicating that road density is not a sufficient proxy for global high-resolution inventories (Gately, Hutyra, and Wing 2015). Carbon Monitor is a global emissions inventory that utilizes a variety of activity data to estimate daily GHG emissions, however the reliance on proprietary traffic data in the ground transportation sector limits the ability to extend to locations where this data is not available (Liu et al. 2020). Other methods have used machine learning (ML) to directly predict emissions, but their ability to generalize globally is unclear (Mukherjee et al. 2021; Scheibenreif, Mommert, and Borth 2021).

JHU/APL has developed an approach to estimate road transportation emissions, and applied this methodology globally. Our "hybrid" algorithm leverages the strengths of ML applied to remote sensing data, in addition to incorporating region-specific emissions factors (EFs) data to create scalable and transparent emissions estimations globally. A detailed description of our method, data sources, and validation results is contained herein.

2 Data and Methods

2.1 Overview

Our hybrid emissions estimation method was primarily composed of three parts: a set of ML models trained to predict road transport activity, an activity estimation pipeline that ensembles, aggregates, and interpolates the ML results, and an emissions factors (EFs) pipeline that converts activity predictions to emissions estimates. This approach combines the strengths of satellite imagery and ML with traditional "bottom-up" emissions inventories that directly incorporate vehicle fleet mix, fuel efficiency, and other EF data. Separating the machine learning and activity estimation from the emission factors pipelines affords continuous improvement of each as newer and better data become available. A high-level system architecture is shown below in Figure 1. A separate method is used to backproject these estimates to historical time periods (2015-2020; see Section 2.3.9).

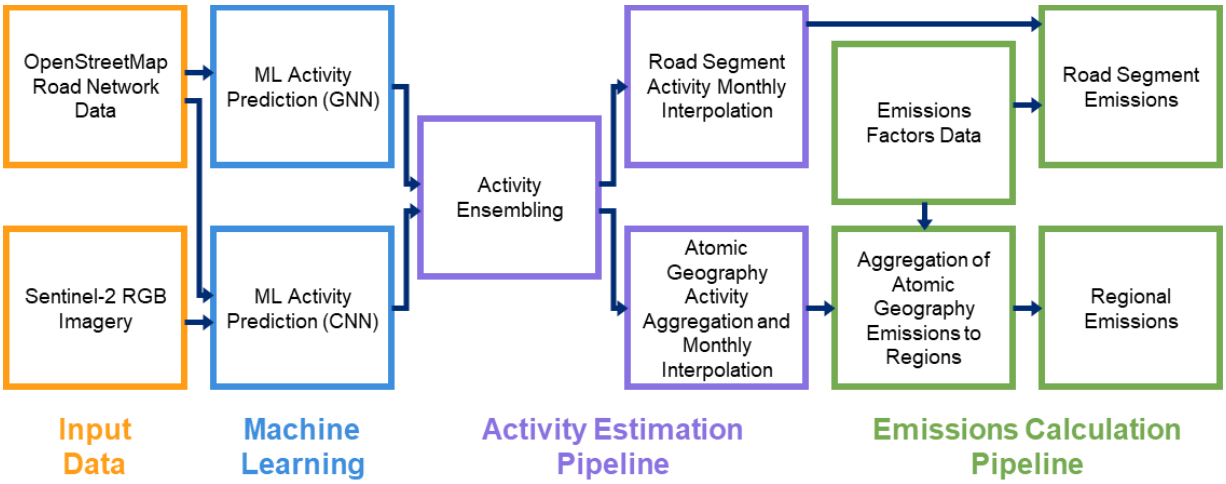

Figure 1 *2021-2024 emissions estimation architecture overview.*

Quarterly remote sensing and geospatial data were fed to two different families of ML models, convolutional neural network (CNN) based models and graph neural network (GNN) based models, producing two separate average annual daily traffic (AADT) estimations on a per-road segment basis. Separate models from each family are used for rural and urban areas, as defined by the European Union Joint Research Center Global Human Settlement Layer Urban Centers Database (GHSL-UCDB) dataset for a globally consistent representation of urban center extent (Florczyk et al. 2019); see Section 2.2.1. Output values from the two different model families were ensembled via averaging within each quarter, and then averaged across quarters within a year to produce a yearly AADT estimate for each road segment (Section 2.4.5). The annual AADT estimate is then converted to the activity value of total vehicle kilometers traveled (VKT) using the known length (capacity) of each road segment. For computational efficiency reasons, the pipeline is then split into two; in one pipeline, the activity estimates per-road segment are interpolated to monthly values, while in the other the activity estimates and capacities are summed

per road type within each atomic geography prior to interpolation. Atomic geographies are non-overlapping geometries that cover the populated landmasses of the world, whose boundaries are the unique combinations of GADM Level-2 boundaries, GHSL-UCDB urban center boundaries, and a half degree latitude/longitude grid; an example of atomic geographies are shown in Figure 2. EFs were computed on a per-atomic geography basis a priori from environmental factors and a curated database of road and vehicle-related factors, assigning EF values to each type of road in an area; Sections 2.2.6 through 2.2.10 describe the data sources used for the factors. Activity values were then multiplied by the appropriate EF for each road type to produce emissions estimates. Emission estimates for the atomic geographies were then aggregated to regions (GADM Levels 0-2) to produce monthly emission estimates from 2021 onward. This process is explained in detail in Section 2.3. Additionally, estimates for 2015-2020 were made by leveraging EDGAR v8.0 data (Crippa et al. 2020) (Section 2.6) to backproject estimates as discussed in Section 2.3.9.

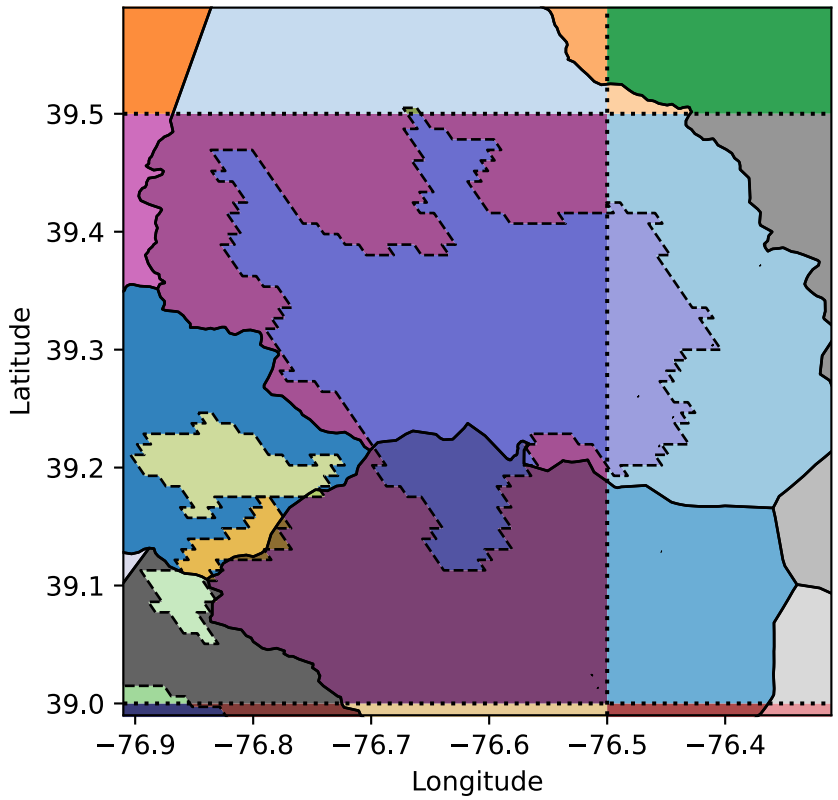

Figure 2 *Example atomic geographies in the Baltimore, Maryland region of the USA. Each color is a different atomic geography; solid lines are GADM Level-2 boundaries, dashed lines are GHSL-UCSB urban center boundaries, and dotted lines are half degree latitude/longitude grid boundaries.*

2.2 Data

2.2.1 Urban Centers

We utilized the European Union Joint Research Center Global Human Settlement Layer Urban Centers Database (GHSL-UCDB) dataset for a globally consistent representation of urban center extent (Florczyk et al. 2019). This database contains approximately 13,000 urban centers worldwide, and utilizes a definition of urban center based on population density and built-up area. Specifically, an urban center was defined as "the spatially-generalized high-density clusters of contiguous grid cells of 1 km^2 with a density of at least 1,500 inhabitants per km^2 of land surface or at least 50% built-up surface share per km^2 of land surface, and a minimum population of 50,000." (Florczyk et al. 2019). Due to this definition, urban center geometries in UCDB often have significantly different shapes and sizes as compared to official administrative bounds of cities, e.g., from OpenStreetMap (OpenStreetMap Contributors 2020) or Global Administrative Areas (GADM) (Global Administrative Areas 2022). Examples of these differences are shown below in Figure 3-Figure 5.

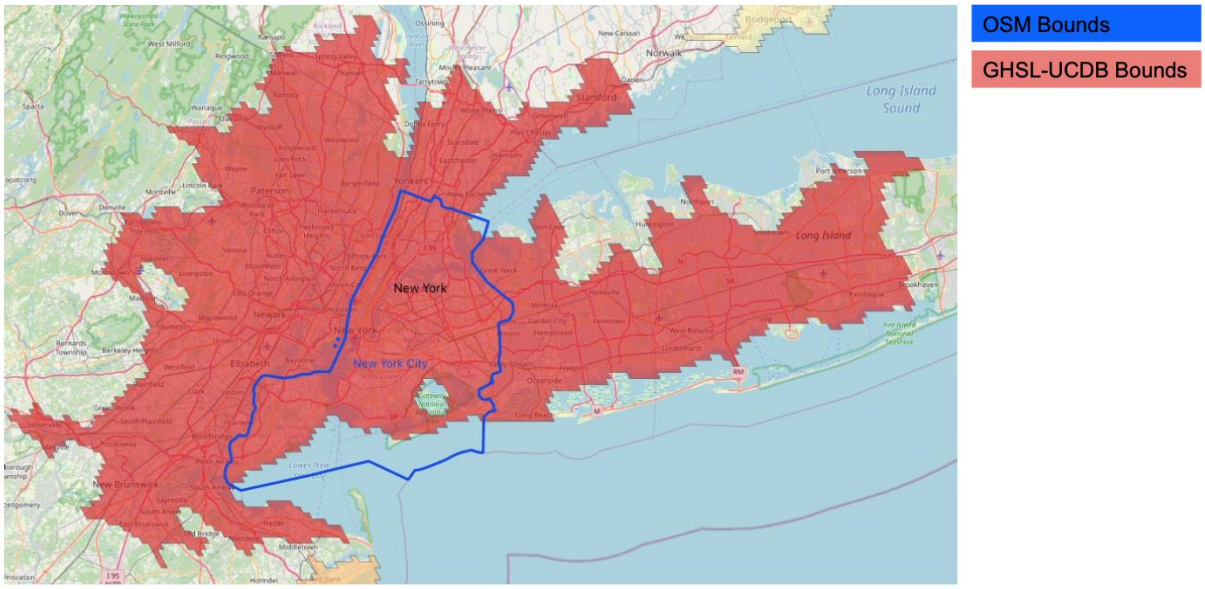

Figure 3 *Comparison of OSM administrative bounds (blue boundary) and GHSL-UCDB city bounds (red area) for New York City, USA*

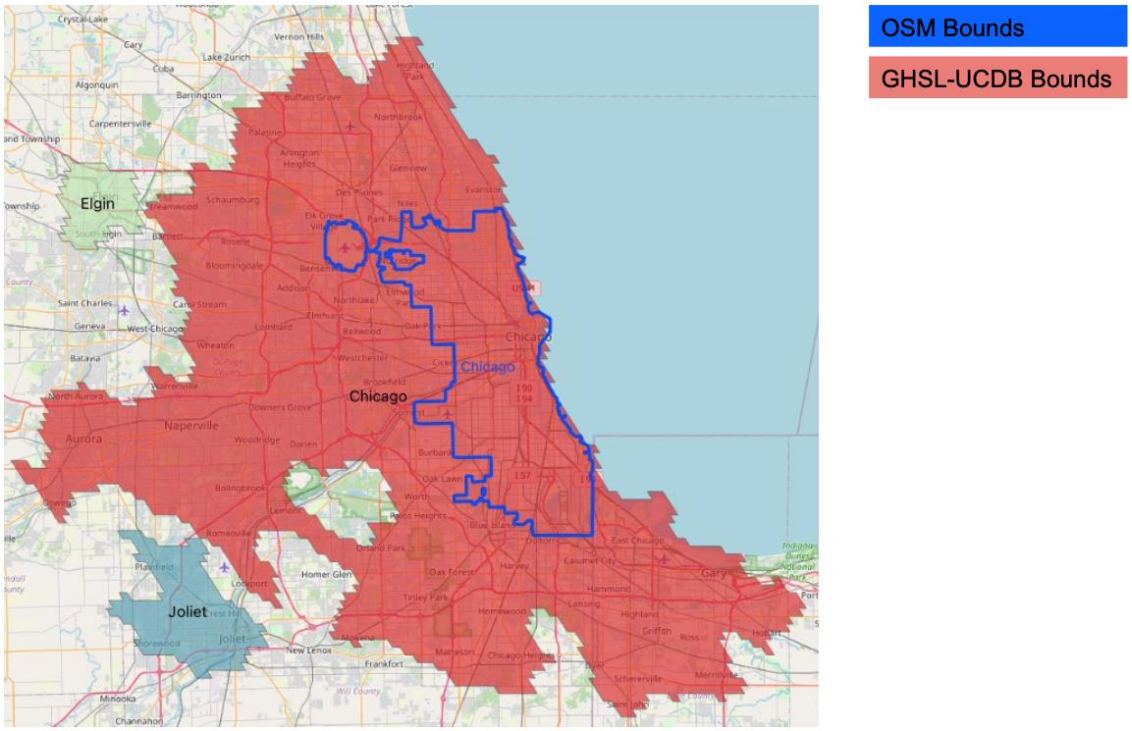

Figure 4 *Comparison of OSM administrative bounds (blue boundary) and GHSL-UCDB city bounds (red area) for Chicago, USA.*

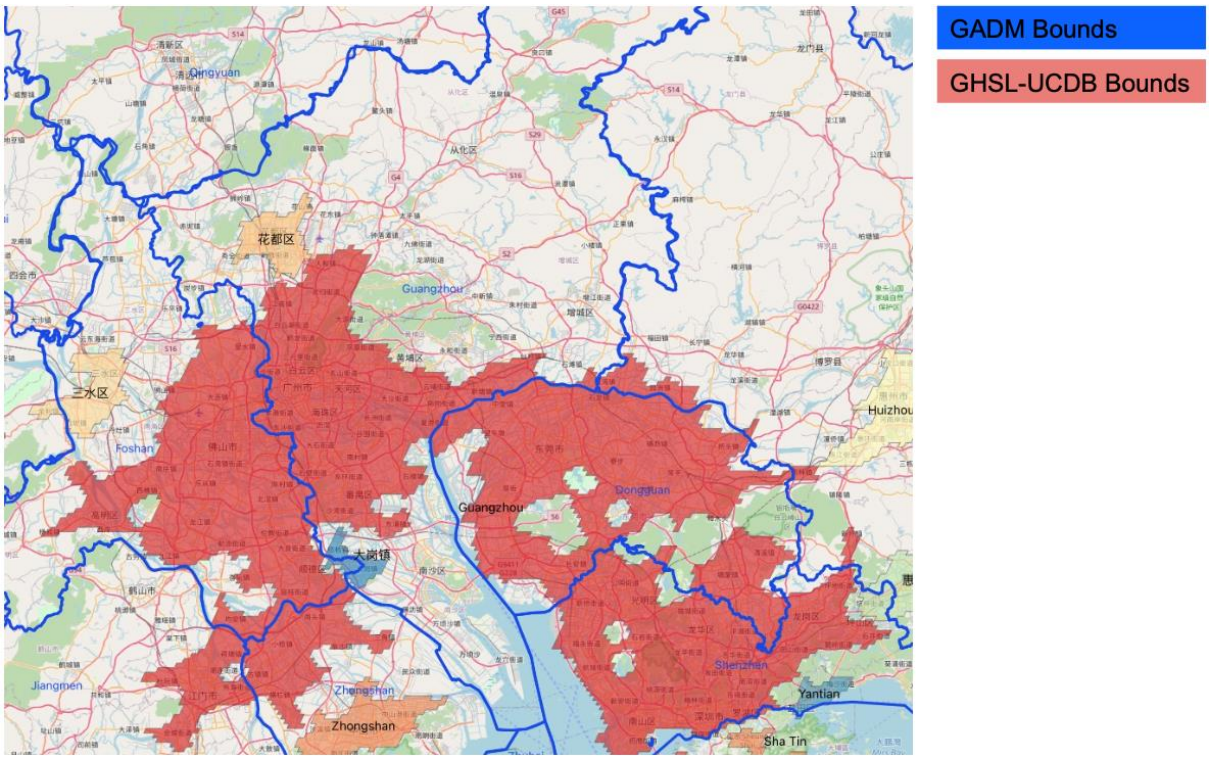

Figure 5 *Comparison of GADM level 2 administrative boundaries (blue boundaries) and GHSL-UCDB urban center bounds (red area) for Guangzhou, China.*

2.2.2 Regional Administrative Boundaries

The Climate TRACE coalition decided to assign emissions based on Global Administrative Areas (GADM) (Global Administrative Areas 2022) at the country (Level 0), state/province (Level 1) and county (Level 2) levels. Here, "county" is the USA based English-version name of the typical administrative area. In other countries, other English-translated names are used. The coalition used a slightly modified version of GADM v4.1; details are described in Section 7.3.

2.2.3 Visual Satellite Imagery

Remote sensing imagery from the Sentinel-2A/B satellites were used as input data in our ML modeling approach to predict road transportation activity (see Section 2.3 below). The European Space Agency's (ESA) Sentinel-2 mission comprises two satellites- Sentinel-2A, launched in 2015, and Sentinel-2B, launched in 2017 (Main-Knorn et al. 2017). Each Sentinel-2 satellite has a 10-day revisit time with a 5-day combined revisit. Both satellites are equipped with a multispectral (MSI) instrument which provides 13 spectral band measurements, blue to shortwave infrared (SWIR) wavelengths (~442 nm to ~2202 nm) reflected radiance. We used the Sentinel-2 Level-2A product at 10 m x 10 m resolution, using bands 4 (red), 3 (green), and 2 (blue) (Drusch et al. 2012).

Sets of images are selected on a per Sentinel-2 Level-2A tile (or granule) basis every quarter, with preference given to unclouded images that best span the tile, with additional unclouded images selected as needed to bring the tile coverage to 90%. If there are insufficient unclouded images, an additional image with up to 10% cloud coverage may be used to improve the tile coverage.

2.2.4 Road Network Data

Using the open-source tools Osmium (Jochen Topf 2023) and OSMnx (Boeing 2017) and custom filters, OpenStreetMap data was filtered to the set of roads that carry normal vehicular traffic (see Section 2.2.6 below for details). A multi-directed graph of the road network was created from that data, and the total edge length (meaning the road length for each direction of traffic is counted separately) was computed to yield the capacity, or road network length, in kilometers. Example road networks for select GHSL UCDB urban centers are visualized in Figure 6. A plot of road network length for differing urban centers is provided in Figure 7; only the top 20 GHSL UCDB urban centers are displayed for visual clarity, though OSM produces road network data outside of urban centers, as well.

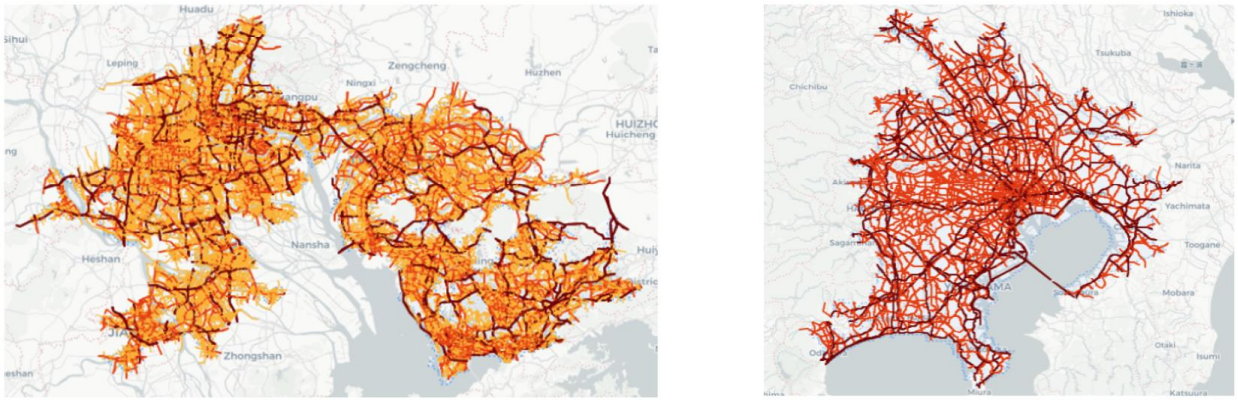

Figure 6 *Example road network data for Guangzhou, China (left) and Tokyo, Japan (right). Highways are in dark red, arterial roads in orange, and local roads in yellow. Local roads are intentionally not displayed for Tokyo due to their large count.*

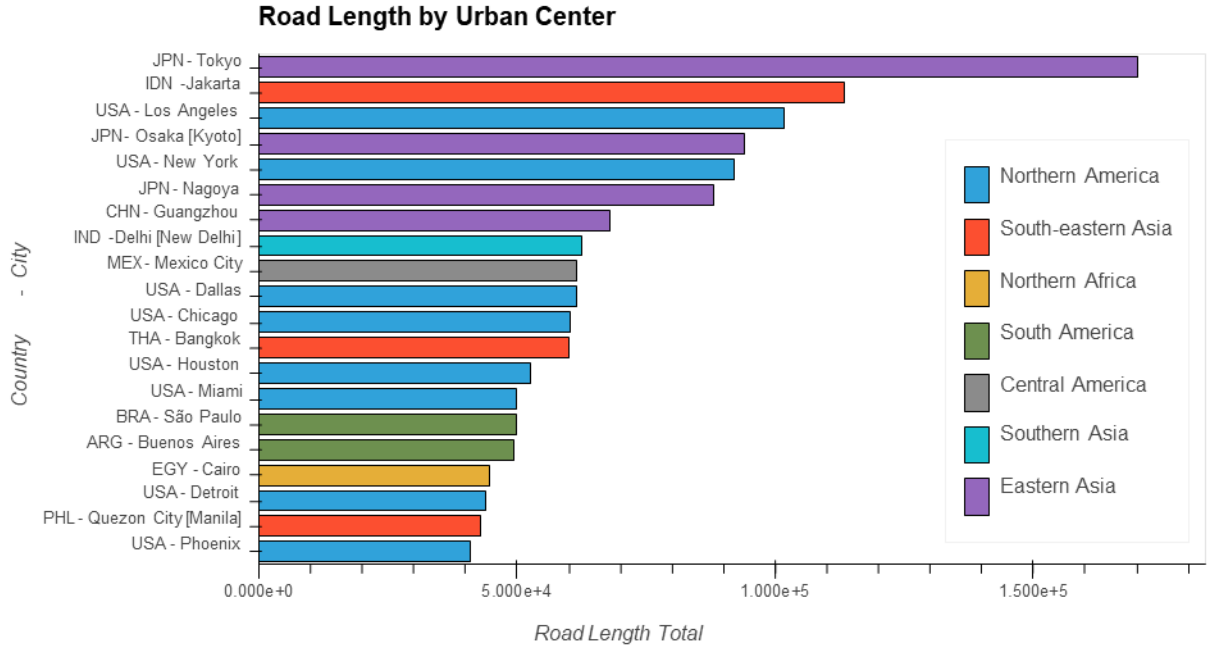

Figure 7 *Total road length for the top 20 GHSL UCDB urban centers ("cities") colored by region.*

Roads and associated metadata (including coordinates, number of lanes, etc.) are constantly changing around the world. OpenStreetMap is updated continuously in an attempt to keep an atlas that reflects reality. While most road segments are consistent between quarters, some road segments appear, some road segments disappear, and some have properties that change. We attempt to deal with these changes by using one snapshot of data from OpenStreetMap per quarter per year. For our activity estimates, we use model inference ensembling to combine four quarters of data; more details are given in Section 2.4.5.

2.2.5 Road Segment Type

Road segment types (categories) were derived from OpenStreetMap data for all public roads. The current supported road types are highway, arterial, and local, which were chosen to align with other similar emissions inventories and traffic-related databases. The mapping between these road types and their respective OSM tags is provided in Table 1. Road type categorization is important in the emissions factor calculation for a given road segment as other emissions factors variables, including vehicle fleet mix and fuel efficiency, could vary significantly across different types of roads. These classes are also used within the modeling effort to distinguish roads (see Section 2.4.2).

Table 1 Road segment type association with OpenStreetMap tags

Road Class	OpenStreetMap Tags
Highway	motorway, motorway_link, trunk, trunk_link
Arterial	primary, primary_link, secondary, secondary_link
Local	tertiary, tertiary_link, residential, living_street, unclassified

2.2.6 Emissions Factors

Calculating emissions factors for a given area was a complex process, due to the fact that an area can actually contain potentially hundreds of thousands of individual road segments, which might be considered "sub-sources". Transportation emissions factors are dependent on many variables, including (but not limited to) road category, vehicle type, fuel type, nominal fuel efficiency and environmental factors. Data collection for each of these variables across the globe was a significant undertaking. Thus, this version of estimated emissions factors focused on collecting data at the country level. A detailed description of the emissions factor calculation is provided in Section 2.3 below. Sources for each type of data required for the emissions factor calculation are shown below in Table 2, with descriptions of each data type provided in subsequent sections.

Table 2 Primary emissions factors data sources used.

Data Type	Source(s)
Road Segment Type	OpenStreetMap (OpenStreetMap Contributors 2020), see Section 2.2.5 above
Vehicle Fleet Mix	Various, see additional information in Section 2.2.7 and Section 6.1
Fuel Type	CURB (World Bank Group 2019), see Section 2.2.8 below
Nominal Fuel Efficiencies	CURB (World Bank Group 2019), see Section 2.2.8 below
Monthly Gridded Temperatures	Climatic Research Unit gridded Time Series v4.07 (Harris et. al. 2020), See Section 2.2.9 below
GHG Emissions Factors	U.S. EPA GHG Emissions Factors Hub (US EPA 2022), see Section 2.2.10 below
Non-GHG Emissions Factors	U.S. DOT Bureau of Transportation Statistics (US BTS 2024), see Section 2.2.10 below

2.2.7 Vehicle Fleet Mix

Vehicle fleet mix refers to the distribution of total vehicles in a given country across various vehicle types. The supported vehicle types were: passenger cars, light duty trucks, single unit trucks, combination trucks, motorcycles, and buses. Country-specific vehicle distribution numbers do not always share these same categories. There might be one, two or more country-specific categories mapping to one supported type or there might be no country-specific category that matches a supported type. These differences were dealt with on a per-country basis. For example, in countries which only reported "trucks" as a single category, we used regional averages of the percentage of trucks in each category to interpolate the single reported category into the three standard truck types.

In general, there are two categories of information available on vehicle fleet mixes: registration data and proportions of kilometers traveled by vehicle category. Our vehicle fleet mix encompasses both types of data and does not distinguish between them in accuracy.

For example, the U.S. Federal Highway Administration (FHWA) provides estimates of both registered cars by state in Table MV-1 (US FHWA 2018) and vehicle-miles traveled in Table VM-

4 (US FHWA 2020). These differ in the percentages of vehicles in each standard type. We would argue that the former (vehicle-miles traveled) is the better distribution of vehicle types to use, as we are attempting to estimate emissions from vehicles actually traveling on roads. However, we have not found such specific information for many countries. Instead, we use the following prioritized list to estimate the vehicle mix in each country:

1. Distribution of vehicle-km traveled categories: as described above
2. Distribution of registration types: as described above
3. Neighboring country average of vehicle fleet mix: use the average vehicle fleet mix from any countries whose GADM Level 0 border touches the target country
4. US FHWA estimate: when all else fails, use the US FHWA estimate for the USA

Country-specific vehicle fleet data was found for 118 countries. A full listing of the countries with country-specific data and their respective sources is provided in the supplementary material (see Section 6.1). Vehicle fleet mix values are currently the same across all supported road types but will be updated as sources of road type-specific data are identified.

For each country with specific vehicle fleet data, when sufficient samples were available, the data was linearly interpolated / extrapolated to cover the modeled time period; otherwise, the data is forward-/backward-filled to cover the time period.

For countries without vehicle specific fleet data, fleet estimates were averaged from any neighboring countries with available data or, failing that, from an average across the UN defined region for the country. For the UN regions of Micronesia and Polynesia, no country data was available, so vehicle fleet data from Melanesia was used as a substitute.

2.2.8 Fuel Type and Nominal Efficiencies

Due to the fact that different fuel types have different emissions factors, it is important to know the relative mix of fuel types for each type of vehicle traveling on a given road segment. The types of supported fuels are:

- Gasoline: no distinction is made between different sub-categories such as (in the US) 87, 89, and 91 octane gasoline or ethanol-free gasoline.
- Diesel: no distinction is made between sulfur-free diesel, bio-diesel or other sub-categories
- Compressed natural gas (CNG)
- Liquefied petroleum gas (LPG)
- Plug-in hybrid: no distinction is made between hybrids that run on different liquid fuels
- Battery electric vehicle (BEV)
- Other fuels (e.g., biogas, ethanol)

The primary source of this data is the Climate Action for Urban Sustainability (CURB) tool (World Bank Group 2019), which provides a global database of fuel type mix by country. Future updates may include updated country or city-specific fuel type data.

CURB was also the primary source of nominal fuel efficiency data for all countries. CURB fuel

efficiency values are reported in units of kilometers per liter and were extracted for all supported fuel and vehicle types described above. Fuel efficiencies were the same across all supported road types (highway, arterial, and local) in this release, but may be continuously updated as better country or region-specific datasets are located.

2.2.9 Fuel Efficiency Environmental Adjustments

Fuel consumption varies under external environmental factors. A study by Lohse-Busch et al., 2013, conducted several tests investigating fuel consumption for several conventional vehicles. These tests included:

- Urban and highway driving tests at 72° F
- Cold urban driving tests at 20° F
- Hot urban driving tests at 95° F and "sunny" skies

These tests broadly found that fuel consumption increases at low temperatures due to heater use and cooler fluids, and fuel consumption also increases at high temperatures due to air conditioning.

The results from the study were grouped by vehicle fuel type and road segment category and averaged to produce representative fuel consumption increases at 20° F and 90° F relative to nominal consumption at 72° F, as listed in Table 3 and Table 4.

Table 3 *Increase in fuel consumption for arterial and local roads. Values were derived from Lohse-Busch et al., 2013, by averaging across UDDS and US06 tests, then averaging across vehicles with the same fuel type.*

Vehicle Fuel Type	Increase at 20° F	Increase at 95° F
Battery Electric	59%	11%
Diesel	7%	25%
Gasoline	5%	20%
Plug-In Hybrid	23%	43%

Table 4 Increase in fuel consumption for highways. Values were derived from Lohse-Busch et al., 2013, by averaging across HWY and US06 tests, then averaging across vehicles with the same fuel type.

Vehicle Fuel Type	Increase at 20° F	Increase at 95° F
Battery Electric	34%	3%
Diesel	4%	16%
Gasoline	5%	14%
Plug-In Hybrid	10%	22%

These fuel consumption increases were used to estimate a temperature-dependent fuel consumption modifier function, with the modifier linearly interpolated from 20° F to 72° and 72° F to 90° F, and values outside that range clipped to the values at the bounds, as shown in Figure 8.

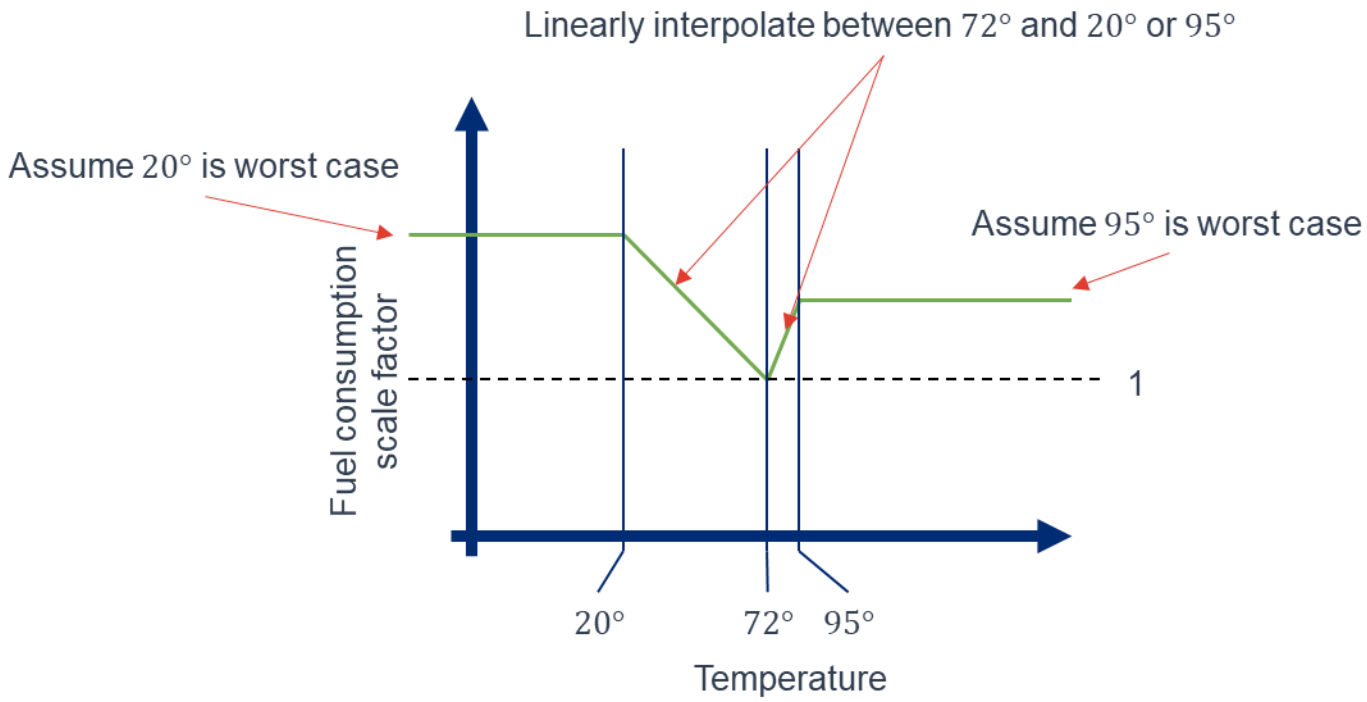

Figure 8 *Design of temperature dependent fuel consumption scale factor function; implemented functions use scale factors found in Table 3 and Table* ***4***

Temperature values on a half degree latitude/longitude grid and monthly basis were pulled from the Climatic Research Unit gridded Time Series (CRU TS) v4.07 dataset (Harris et. al. 2020). We used this dataset due to its standard usage in the literature; the 2020 paper and the 2014 paper for v3.x of the dataset have been cited nearly 7,000 times together. The dataset includes temperatures from 1901 to 2022; the values from 2022 were repeated to provide temperature estimates for 2023 and 2024. Version 4.08 of the dataset was released after it had been incorporated into our estimation workflow. This updated dataset includes temperature estimates for 2023.

2.2.10 Vehicle GHG and non-GHG Emissions Factors

GHG emissions factors refer to how much of a given greenhouse gas is emitted per unit of fuel burned and varies by fuel type. Our data focuses on carbon dioxide (CO_2), nitrous oxide (N_2O), and methane (CH_4) emissions factors, using data from the U.S. Environmental Protection Agency (US EPA 2024).

For nitrous oxide and methane, the emissions factors for each gas were given in units of grams of each gas per mile driven. This led to a different emission factor calculation for these gases than for carbon dioxide; details are given in Section 2.3.

Emission factors for non-GHGs follow a similar methodology as nitrous oxide (N_2O) and methane emissions using data immediately sourced from the U.S. DOT Bureau of Transportation Statistics (US BTS 2024), though ultimately derived from the U.S. EPA. The non-GHGs estimated include other nitrogen oxides (NOx), carbon monoxide (CO), particulate matter ($PM_{2.5}$), and other non-

GHG hydrocarbons (HC). $PM_{2.5}$ emissions are provided both as a total and broken out as separate contributions from brakewear, tirewear, and exhaust.

2.3 Emissions Calculations

The road transportation sector reports emissions, emissions factor, activity, capacity, and capacity factor on a per month and per GHG basis for GADM Level 1 and GADM Level 2 regions, and on an annual and per greenhouse gas basis for GADM Level 0 regions. These variables are defined at different levels, from individual road segments to GADM Level 0, and are defined in the following sections such that the following general equations hold true:

- **Emissions** = **Activity** * Emissions Factor
- **Activity** = **Capacity** * Capacity Factor

Values in **bold** are considered the independent variables, with calculations defined in more detail in Sections 2.3.1 through 2.3.6, while dependent variables are described in more detail in Section 2.3.8.

2.3.1 Region Emissions

Road transportation emissions (E) are reported on a monthly basis for GADM Level 1 (state/province) and GADM Level 2 (county) regions, and on an annual basis for GADM Level 0 (country) regions. Emissions are calculated by summing over the emissions for the atomic geographies within each region r, where atomic geographies are unique combinations of GADM Level 2 areas, GHSL UCDB urban areas (or no urban area), and a half degree global grid. The sum for GADM Level 0 regions is:

$$E_{r,g,y} = \sum_{a \in r, j \in y} AE_{a,g,j} \quad (1)$$

for GADM Level 0 regions, where $AE_{a,g,j}$ is the road transportation emissions (AE) for each GHG g (or other non-GHG emission) for month j for an atomic geography area a and y is the year. Emissions for GADM Level 1 and 2 regions are similar:

$$E_{r,g,\mathrm{j}} = \sum_{a \in r} AE_{a,g,j} \quad (2)$$

Emissions ($E_{r,g,j}$, $E_{r,g,y}$) are reported in units of metric tonnes (per month or year).

2.3.2 Atomic Geography Emissions

Total road transportation emissions (AE) for each GHG g (or other non-GHG emission) for month j for an atomic geography area a could be calculated as:

$$AE_{a,g,j} = \sum_{i \in a} SE_{g,i,j} \quad (3)$$

where $SE_{g,i,j}$ is the "segment emissions" for a road segment i, and the sum is over any road segment which is contained by the atomic geography area a. Each $SE_{g,i,j}$ is calculated as:

$$SE_{g,i,j} = \alpha \cdot N_j \cdot AADT_{i,j} \cdot l_{i,j} \cdot SEF_{g,i,j} \quad (4)$$

where:

- α is an activity scale factor to align emissions with EDGAR estimates (See Section 2.3.7)
- N_j is the number of days in month j
- $AADT_{i,j}$ is the average annual daily traffic of the road segment i for month j, in units of vehicles per day (See Section 2.4.5)
- $l_{i,j}$ is the length of the road segment i in month j, in units of kilometers
- $SEF_{g,i,j}$ is the segment emission factor for greenhouse gas g, road segment i and month j in units of mass per vehicle kilometer

However, this formulation is somewhat computationally inefficient, with a computational complexity of $O(G * I)$, where G is the number of gases (on the order of 10) and I is the number of road segments (on the order of 4e8 globally). A more computationally efficient approach $O(I)$ calculates emissions as:

$$AE_{a,g,j} = \sum_{c} CACT_{a,c,j} * CEF_{a,c,g,j} \quad (5)$$

where $CACT_{a,c,j}$ is the monthly activity within the atomic geography per road-segment category c, and $CEF_{a,c,g,j}$ is the monthly road-segment category emission factor (Section 2.3.3). Each $CACT_{a,c,j}$ is calculated as:

$$CACT_{a,c,j} = \alpha \cdot N_j \cdot \sum_{i \in a,c} AADT_{i,j} \cdot l_{i,j} \quad (6)$$

And $CEF_{a,c,g,j}$ is equivalent to $SEF_{g,i,j}$ where c is the road segment category of i and a is the atomic geography that contains i.

2.3.3 Segment Category Emission Factor

Emission factors are currently calculated in two different paths, as the source emission factors from the EPA are expressed in units of <mass>/<volume fuel> for carbon dioxide, and units of <mass>/<distance traveled> for other greenhouse and non-greenhouse gases.

For carbon dioxide, the emission factor for each road segment category is calculated as:

$$CEF_{a,g=CO_2,c,j} = \sum_{f} t_{a,c,j,f} \cdot \left(\sum_{v} \eta_{a,v,f} \cdot m_{a,j\in y,v,f} \cdot eg_{j\in y,v,f} \right) \quad (7)$$

- $\eta_{a,v,f}$ is the fuel efficiency, in units of liters of fuel per km, for a vehicle type v, fuel type f, and atomic geography a. Fuel efficiencies are currently estimated on a per-country basis (Section 2.2.8).
- $m_{a,j\in y,v,f}$ is the vehicle mix, as a fraction, typically present in atomic geography a based on the vehicle type v, fuel type f, and year y of month j. Specifically, we require that $\sum_{v,f} m_{a,j,v,f} = 1$. Vehicle mix is estimated on an annual per-country basis (Section 2.2.7).
- $egv_{j\in y,v,f}$ is the CO2 emissions factor, in grams of CO2 per liter of fuel, for the vehicle type v, fuel type f, and year y of month j. The CO2 emissions factor is estimated on an annual basis (Section 2.2.10).
- $t_{a,c,j,f}$ is a unitless, temperature-dependent and road-segment category-dependent modifier to fuel efficiency. It is calculated on a monthly, half-degree grid basis (Section 2.2.9).

For other greenhouse and non-greenhouse gases, the emission factors are independent of road segment category and are calculated on an annual basis as follows:

$$CEF_{a,g\neq CO_2,c,j} = \sum_{v,f} m_{a,j\in y,v,f} \cdot egd_{g,j\in y,v,f} \quad (8)$$

where $egd_{g,j\in y,v,f}$ is the gas emissions factor, in grams of gas per vehicle kilometer, for the vehicle type v, fuel type f, and year y of month j (Section 2.2.10). The gas emissions factors are estimated on an annual basis.

2.3.4 Capacity

Capacity is simply defined as the total length of the road network in an asset area for month j for any region r:

$$CAP_{r,j} = \sum_{a\in r} ACAP_{a,j} \quad (9)$$

where $ACAP_{a,j}$ is the atomic geography road segment capacity in units of kilometers, and is given as:

$$ACAP_{a,j} = \sum_{i\in a} l_{i,j} \quad (10)$$

Similarly, we can define a capacity for any given road segment i as $SCAP_{i,j}$:

$$SCAP_{i,j} = l_{i,j} \tag{11}$$

Note that because OSM data (Section 2.2.4) can change over time, it is possible for length (and therefore capacity) of a road segment to also change over time.

2.3.5 Activity

Activity (ACT) for any region r is the number of vehicle kilometers traveled in month j:

$$ACT_{r,j} = \sum_{a \in r} AACT_{a,j} \tag{12}$$

where

$$AACT_{r,j} = \alpha \cdot N_j \cdot \sum_{i \in a} AADT_{i,j} \cdot l_{i,j} \tag{13}$$

For segment level activity, we similarly define $SACT_{i,j}$:

$$SACT_{i,j} = \alpha \cdot N_j \cdot AADT_{i,j} \cdot l_{i,j} \tag{14}$$

2.3.6 Segment Capacity Factor

Only the *segment* capacity factor is independent, the region capacity factor is defined in Equation 19 below. The segment capacity factor (SCF) is defined as the ratio of activity to capacity:

$$SCF_{i,j} = \frac{SACT_{i,j}}{SCAP_{i,j} \cdot N_j} \tag{15}$$

$$SCF_{i,j} = \frac{\alpha \cdot N_j \cdot AADT_{i,j} \cdot l_{i,j}}{l_{i,j}} = \alpha \cdot N_j \cdot AADT_{i,j}$$

This variable provides a direct view into the predicted AADT.

2.3.7 Activity Scale Factor

To better align our estimates with EDGAR v8.0 (Crippa et al. 2020, Section 2.6), an activity scale factor was introduced. While a portion of the difference between EDGAR and our estimates may ultimately be due to emission factors, due to biases in the training data (Section 2.4.1) our raw, region activity estimates are expected to be high, so the scale factor was chosen to be introduced to the activity component of the emissions estimation. The scale factor is calculated as follows:

$$\alpha = \frac{\sum_{r,y} G_{r,y}}{\sum_{r,y} \hat{E}_{r,CO2,y}} \tag{16}$$

Where $\hat{E}_{r,CO2,y}$ are our annual GADM Level-0 CO_2 emission estimate calculated with an initial activity scale factor of 1, and $G_{r,y}$ are the annual country level EDGAR v8.0 road transportation CO_2 emission estimates. The sums are over the countries and years (2021 and 2022) in common between our estimates and EDGAR v8.0. Using this methodology, the activity scale factor was calculated to be 0.3255.

2.3.8 Dependent Variables

The reported region emissions factors (EF) are defined as the emissions divided by the activity for greenhouse gas g in month j for any aggregation area a:

$$EF_{r,g,j} = \frac{E_{r,g,j}}{ACT_{r,j}} \tag{17}$$

This can equivalently be viewed as a segment activity-weighted average emissions factor:

$$EF_{r,g,j} = \frac{\alpha \cdot N_j \cdot \sum_{i \in r} AADT_{i,j} \cdot l_{i,j} \cdot SEF_{g,i,j}}{\alpha \cdot N_j \cdot \sum_{i \in r} AADT_{i,j} \cdot l_{i,j}} \tag{18}$$

The reported region capacity factor (CF) is defined as the activity in month j (ACT_j) divided by capacity (CAP_j) for any region r:

$$CF_{r,j} = \frac{ACT_{r,j}}{CAP_{r,j}} \tag{19}$$

This can equivalently be viewed as a segment length-weighted average of vehicles per month:

$$CF_{r,j} = \frac{\alpha \cdot N_j \cdot \sum_{i \in r} AADT_{i,j} \cdot l_{i,j}}{\sum_{i \in r} l_{i,j}} \tag{20}$$

2.3.9 Emissions Backprojection

Our current methodology would have several challenges to overcome if it was to be applied to periods before 2021. Due to its crowd-sourced nature, OSM data coverage and quality decreases the farther back in time one looks. Additionally, the time period covering the response to the COVID-19 pandemic in 2020 is also expected to challenge our methodology, as no direct indicators of traffic volume during that time were used. Instead, in order to provide historical, country level (GADM Level-0) emission estimates back to 2015, EDGAR v8.0 data was used as a basis to anchor emission estimates.

For those countries that were included in the EDGAR v8.0 dataset (as identified by their ISO-3 country code, see Section 7.3), historical estimates are given as follows:

$$E_{r,g,y'} = \left(\frac{G_{r,y'}}{\frac{1}{2}\sum_{y=2021,2022} G_{r,y}} \right) \left(\frac{1}{2} \sum_{y=2021,2022} E_{r,g,y} \right) \tag{21}$$

Where the first term is the ratio between the EDGAR v8.0 CO_2 emissions for the historical year y' and the average annual CO_2 emissions for 2021-2022, and the second term is the average estimated GHG or non-GHG emissions for gas g over the same time period.

For those countries that are omitted from the EDGAR v8.0 dataset, historical estimates are instead given by:

$$E_{r,g,y'} = \left(\frac{\sum_r G_{r,y'}}{\frac{1}{2}\sum_{r,y=2021,2022} G_{r,y}}\right)\left(\frac{1}{2}\sum_{y=2021,2022} E_{r,g,y}\right) \quad (22)$$

Where the first term is now the ratio between the global total of EDGAR v8.0 CO_2 emissions for the historical year y' and the average global annual CO_2 emissions for 2021-2022.

2.4 Machine Learning Models

As part of our hybrid modeling approach, machine learning (ML) models were trained to predict road activity from satellite imagery and road network data. These predictions were required in the absence of global, openly available, and high-quality traffic activity data and is a significant departure from existing methods.

2.4.1 Ground Truth Road Activity Data

To train our ML models, we utilized the U.S. Highway Performance Monitoring System Average Annual Daily Traffic (AADT) data from 2017 and 2018 (US FHWA 2017). This AADT data was recorded using road-side devices and was provided by each state independently. We utilized the total AADT measure in our work, measured in vehicles per day. AADT data was not available for every road segment and was typically only recorded on major highways and arterial (collector) roads. Where possible, the AADT values are aligned to OSM roads to use as ground truth when training the neural networks.

2.4.2 Convolutional Neural Network (CNN)

Our first machine learning approach used semantic segmentation CNNs to predict AADT. Specifically, we input visual satellite imagery in combination with rasterized road network data to predict AADT on a per-pixel basis (Figure 9). This approach was informed by previous work in directly regressing road transport CO_2 emissions (Mukherjee et al. 2021). Models were trained using the Sentinel-2 Level-2A product at 10 m x 10 m resolution, using bands 4 (red), 3 (green), and 2 (blue) (Drusch et al. 2012), and separate models were trained and used on urban and non-urban areas respectively (Section 2.2.1).

Road network data was retrieved from OpenStreetMap and rasterized for the corresponding extent of each visual image tile. Each standardized road type (*highway*, *secondary*, *local*, see Sections 2.2.4 and 2.2.5) was rasterized independently, and the resulting raster channels are concatenated together to form a three-channel image. This image was then combined with the visual image to form a six-channel input image that was input to the CNN. Thus, the CNN model is tasked with predicting the number of vehicles traveling on a road segment as a function of visual satellite image features and road location and type information. We primarily used MAnet-based architectures (Fan et al. 2020) for our segmentation models, based on the findings of similar previous work (Mukherjee et al. 2021).

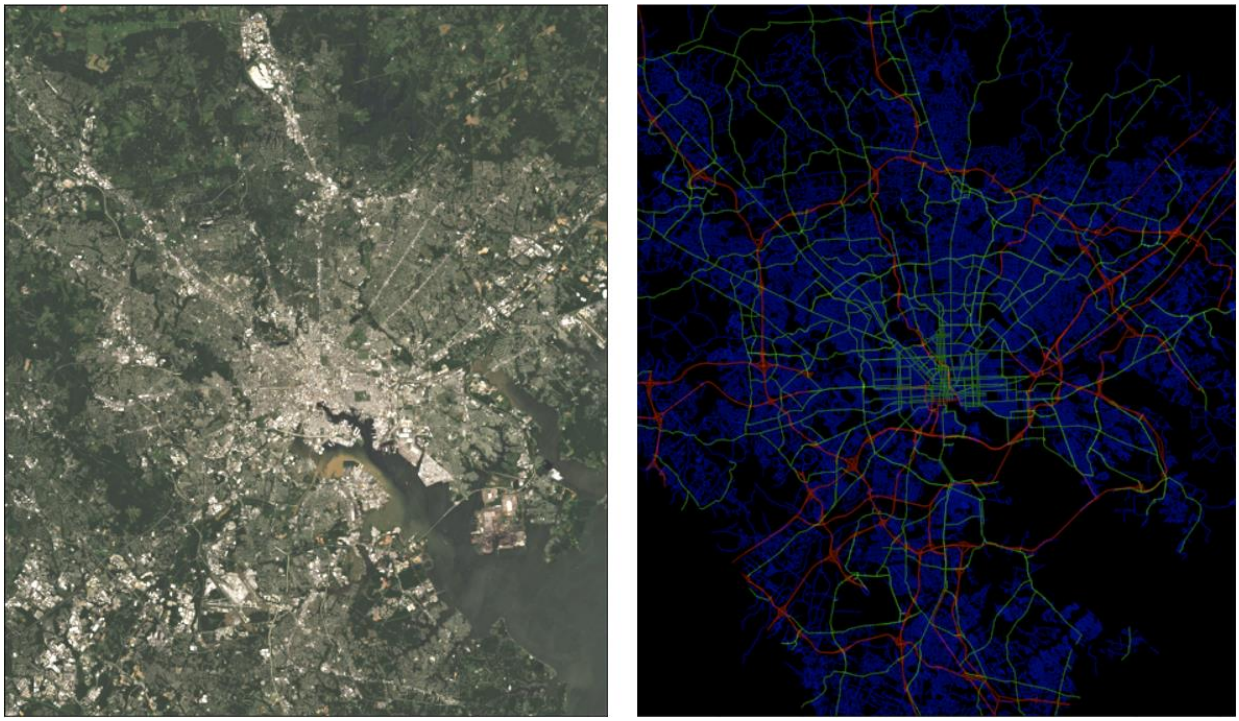

Figure 9 *Example Sentinel-2 visual (RGB) satellite image (left) and corresponding rasterized OSM road network data (right) for Baltimore, Maryland USA. The OSM raster colors represent different road types: highways (red), secondary roads (green), and local roads (blue).*

When the model was used within the overall emissions calculation pipeline, pixel-based AADT predictions were post-processed to associate predicted values with their corresponding road segment. Ten evenly spaced locations along the length of each road segment were selected to measure the AADT prediction; locations that were not marked as cloudy by the Sentinel-2 Level-2A scene classification map were averaged to produce a single AADT value for that road segment within each image; these AADT values were then averaged across all images within the quarter to produce the final prediction for the CNN models.

The loss function used to train the model has two components, the first of which is a fully-supervised mean square log error term calculated on unclouded pixels containing nonzero truth AADT values. Log predictions and errors are used to account for the many orders of magnitudes AADT values span. The second component is a semi-supervised loss term to address locations where the truth AADT is zero. For this loss term, the same image is passed through the model multiple times using different flips/rotations, and the loss then seeks to reduce the variance between the pixel level AADT predictions after undoing those flips/rotations.

2.4.3 Graph Neural Network (GNN)

Another type of ML model trained to predict AADT was graph neural networks (GNNs) (Bronstein et al. 2017). Road networks inherently take the form of a graph structure, and GNNs

can capture road activity across a range of scales more easily than the image-based convolutional neural network (CNN) segmentation models. CNN-based solutions constrain the spatial area that can be covered during inference, making it difficult to capture potential dependencies on features in neighboring or distant locations. GNNs can easily leverage various features assigned to nodes and efficiently reason over the full road network graph to provide more robust predictions of on-road activity.

For this work, a GNN was trained using OpenStreetMap road network data, including a number of road features: the number of lanes, road length, road type, link or not (such as an exit ramp), and the directional angle between roads. Separate models were trained for both urban and non-urban areas (Section 2.2.1). The Graph Attention v2 (GATv2) network (Brody et.al. 2021) architecture was used as it allows for both edge and node input features, and was set up to predict log-AADT values. We note that the GNN does not use visual imagery as input and is able to learn a relationship between road types and configurations to the density of traffic on those roads.

The loss function used to train the GNN network, like the CNN network, also has two components; the first is a fully-supervised L1 loss on the log error of AADT values (for road segments with AADT truth values), and the second is a semi-supervised relative consistency loss. The consistency loss is computed per-intersection, and is formulated as the net traffic flow into an intersection (i.e., sum of predicted AADT for road segments entering the intersection minus the sum of predicted AADT for road segments exiting the intersection) divided by the average flow through the intersection (i.e., the average of the sum of predicted AADT for road segments entering and the sum for roads exiting the intersection).

2.4.4 Model Training Datasets

Training data was increased compared to previous years to include rural areas for training GNN and CNN models targeted to rural areas. Table 5 shows the details of the various data sources used for training the GNN and CNN models. A late bug was uncovered that revealed the rural models were mostly only trained on OSM networks and AADT data from the fourth quarter of 2018 (2018 Q4), with a small amount of data from 2017 Q4; this will be corrected in future data releases, and is expected to improve the accuracy of our activity prediction in rural areas.

Table 5 *Training details and comparison between the 2023 and 2024 release of the road transportation emissions datasets*

Model	***Training Data***	**2023 Dataset**	**2024 Dataset**
GNN-Urban	*US HPMS AADT*	2017 and 2018	2017 and 2018

Model	*Training Data*	2023 Dataset	2024 Dataset
	OpenStreetMap Dataset Date	4 quarters each in 2017 and 2018	4 quarters each in 2017 and 2018
	Areas	308 urban areas for each quarter of 2017, and 307 urban areas for each quarter of 2018; total 2460 samples	305 urban areas for each quarter of 2017, and 311 urban areas for each quarter of 2018; total 2464 samples
GNN-Rural	*US HPMS AADT*	N/A	2017 and 2018
	OpenStreetMap Dataset Date	N/A	2017 Q4 and 2018 Q4
	Areas	N/A	1148 rural areas for 2018 Q4 and 142 rural areas for 2017 Q4; areas are aligned to Sentinel-2 tiles
CNN-Urban	*US HPMS AADT*	2017 and 2018	2017 and 2018
	Sentinel-2 Imagery	One image per urban area, per quarter for a total of 2028 images	Nominally one image per tile with urban areas per quarter (some locations have multiple images to ensure close to full coverage after taking into consideration clouds), for a total of 2438 images
	OpenStreetMap Dataset Date	4 quarters each in 2017 and 2018	4 quarters each in 2017 and 2018
	Areas	308 urban areas for each quarter of 2017, and 307 urban areas for each quarter of 2018; total 2460 samples	252 tiles covering 308 urban areas

Model	*Training Data*	2023 Dataset	2024 Dataset
CNN-Rural	*US HPMS AADT*	N/A	2017 and 2018
	Sentinel-2 Imagery	N/A	Nominally one image per tile per quarter (some tiles have multiple images to ensure close to full coverage after taking into consideration clouds), for a total of 11927 images
	OpenStreetMap Dataset Date	N/A	2017 Q4 and 2018 Q4
	Areas	N/A	1152 tiles using 2018 Q4 OSM data and 141 tiles using 2017 Q4 OSM data; areas are aligned to Sentinel-2 tiles and cover the United States

2.4.5 Model Inference & Ensembling

The data sources for inference has expanded greatly compared to previous years due to covering additional years and all global regions. In Table 6 we highlight the differences between the 2023 dataset release and the current 2024-year data release.

Table 6 *Inference details and comparison between the 2023 and 2024 road transportation emissions dataset releases.*

Model	*Inference Data*	2023 Dataset	2024 Dataset
GNN-Urban	*OpenStreetMap Dataset Date*	4 quarters each in 2021 and 2022 covering 10k urban areas	15 quarters between 2021 Q1 and 2024 Q3 covering almost 13k urban areas
GNN-Rural	*OpenStreetMap Dataset Date*	N/A	15 quarters between 2021 Q1 and 2024 Q3, broken into approximately 15k rural road networks per quarter

Model	*Inference Data*	2023 Dataset	2024 Dataset
CNN-Urban	*OpenStreetMap Dataset Date*	4 quarters each in 2021 and 2022 covering 10k urban areas	15 quarters between 2021 Q1 and 2024 Q3 covering almost 13k urban areas
	Sentinel-2 Imagery	A total of 37885 images covering 10k urban areas spread over the 8 quarters of 2021 and 2022 (multiple urban areas can be covered by the same image, and multiple images may be needed to cover a single urban area)	A total of 67424 images covering almost 13k urban areas over the 15 quarters between 2021 Q1 and 2024 Q3 (multiple urban areas can be covered by the same image, and multiple images may be needed to cover a single urban area)
CNN-Rural	*OpenStreetMap Dataset Date*	N/A	15 quarters between 2021 Q1 and 2024 Q3, broken into approximately 15k rural road networks per quarter, one per Sentinel-2 tile
	Sentinel-2 Imagery	N/A	A total of 315668 images covering almost 19k tiles over the 15 quarters between 2021 Q1 and 2024 Q3 (approximately 4k tiles do not actually contain roads)

For each area (urban or rural), for each year, we ended up with up to eight predictions of AADT for every road segment; 2024, having only three quarters of available data, has a maximum of six predictions. However, as discussed in Section 2.2.4, OpenStreetMap data is continuously updated, and so not every road-segment is present across all eight predictions (four from the CNN, four from the GNN). Additionally, some CNN predictions were not possible due to persistent cloud cover. To create a more robust and predictive yearly AADT prediction model, ensembling was performed using the CNN and GNN models.

To ensemble the eight, possibly non-identical, sets of road-segment AADT predictions, we employed the following routine:

1. For each model, each AADT prediction for an OSM road segment was assigned to possibly multiple atomic road segments. Atomic road segments were OSM road segments that have

been split at our atomic geographies; the unique ID of an atomic road will change if the underlying OSM road changes in either geometry or metadata.

2. For each model, the atomic road AADT predictions within a year were averaged together
3. The yearly atomic road AADT predictions for each model were then averaged together. For cases where a road is only present in the GNN due to clouds in the CNN image, this effectively sets the data for that segment to the mean GNN predicted value

The daily activity estimates (AADT * road length) and capacities (road lengths) were then aggregated within each atomic geography by road segment category to produce annual estimates. In the aggregation, the contribution from each atomic road segment is weighted by the portion of each year each atomic road segments is valid for (e.g., a road segment that is only valid for the first quarter will only contribute about ¼ of its values to the total). This effectively weighs the road segments that only appear in one quarter as contributing lower to our estimate of emissions than road segments that are present in all four quarters.

From these daily activity and capacity at yearly intervals, we linearly interpolate to produce estimates at monthly intervals. Months before July 2nd 2021 or after May 2nd, 2024 ((halfway between January 1st and September 1st 2024) were backward/forward filled from the nearest estimate.

An example ensemble AADT output from the 2023 dataset can be seen below in Figure 10.

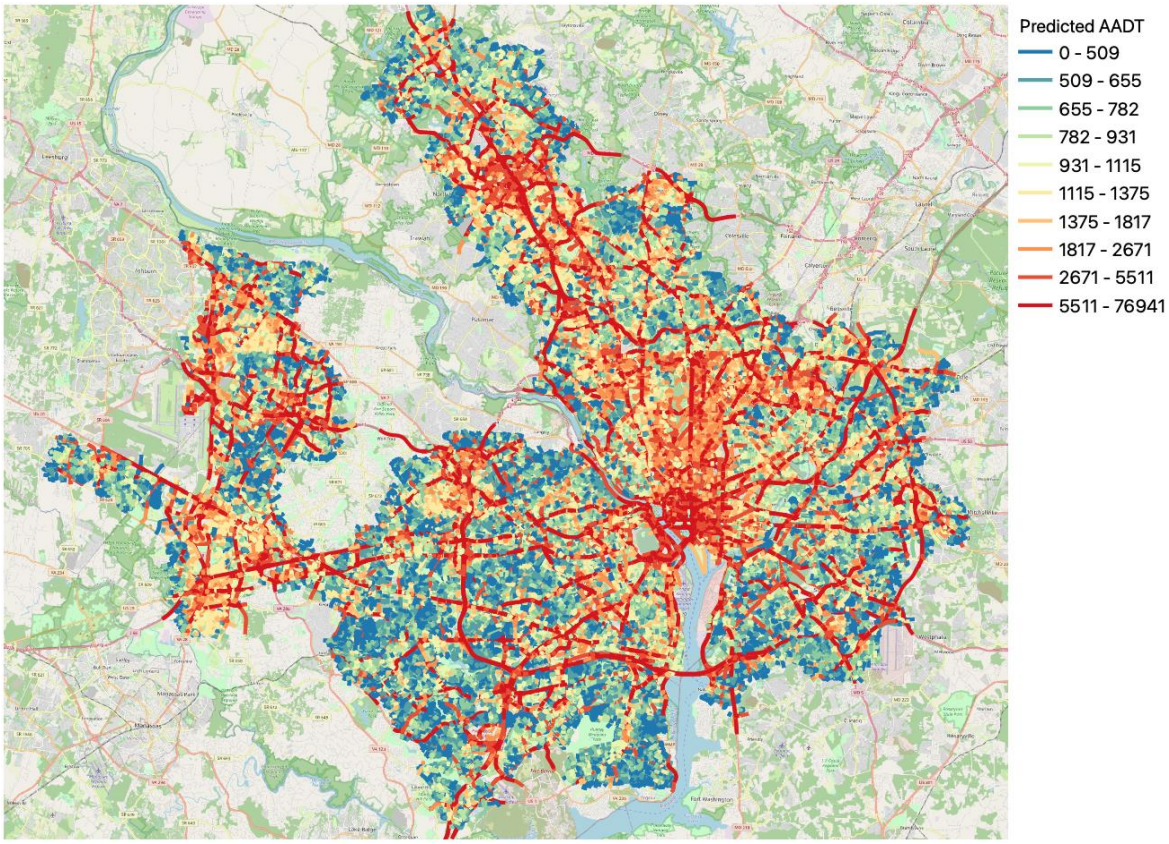

Figure 10 *Ensemble-predicted AADT for 2021, measured in vehicles per day, for Washington, D.C. Cooler colored road segments indicate relatively less AADT compared to warmer colored road segments.*

2.5 Uncertainty & Confidence

This 2024 dataset release also includes a first estimate of the uncertainty in our emissions estimates along with a confidence level for that uncertainty. In this section, we discuss our methods for quantifying uncertainty in assets, reported as percentage.

2.5.1 Uncertainty Overview

In addition to CO_2, N_2O, and CH_4 emissions estimates, we provide estimates of activity, capacity, and other values. A full dataset description is in Section 6.2. In Table 7 below, we summarize the approach taken to estimate the uncertainty in each value.

In the following subsections, we provide details on the estimation process in detail.

Table 7 *Summary of methods to estimate uncertainty per column*

Column	Method
capacity	Estimate from https://github.com/microsoft/RoadDetections
activity	Monte Carlo simulations
CO2_emissions_factor	Propagation of error from CO2_emissions and activity
CH4_emissions_factor	Propagation of error from CH4_emissions and activity
N2O_emissions_factor	Propagation of error from N2O_emissions and activity
other_gas_emissions_factor	Propagation of error from other_gas_emissions and activity
CO2_emissions	Monte Carlo simulations
CH4_emissions	Monte Carlo simulations
N2O_emissions	Monte Carlo simulations
other_gas_emissions	Monte Carlo simulations
total_CO2e_100yrGWP	Propagation of error from CO2_emissions, CH4_emissions, and N2O_emissions, including constants
total_CO2e_20yrGWP	Propagation of error from CO2_emissions, CH4_emissions, and N2O_emissions, including constants

2.5.2 Coefficient of Variation

Our first assessment of emissions variability is via the coefficient of variation,

$$CV(E_{g,j}) = \frac{std_r(E_{r,g,j})}{mean_r(E_{r,g,j})} \tag{23}$$

where $E_{r,g,j}$ corresponds to the emissions of gas g in month j in all regions in region r. The coefficient of variation has been applied to uncertainty analyses in road emissions in the literature. At the UN region level, the coefficient of variation suggests that while CO_2 emissions are often the largest, this does not necessarily correspond to the largest variation (Figure 11). In particular, CH_4 is more likely to have a larger coefficient of variation. The figure shows just three regions; the rest of the data is plotted in Section 6.3 as Figure 27.

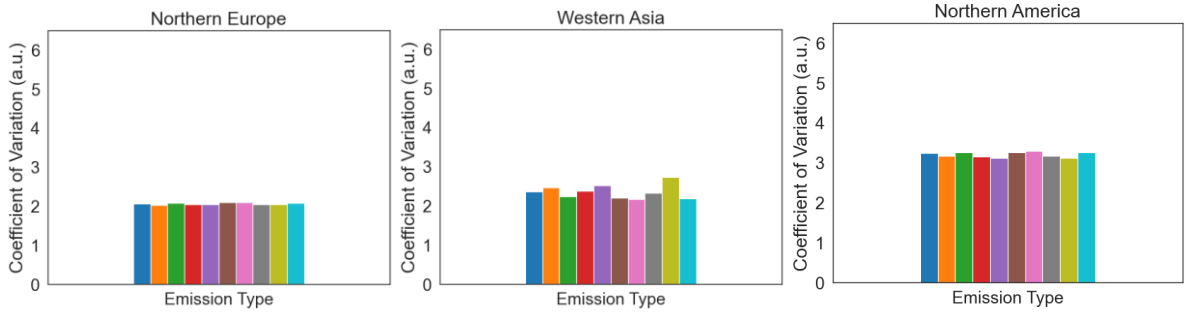

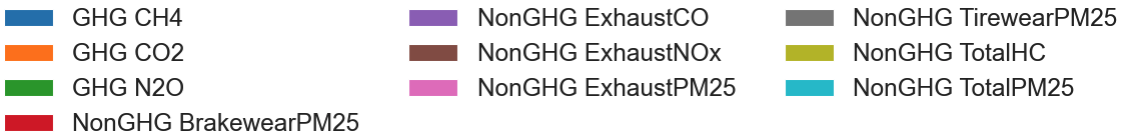

Figure 11 *Coefficient of variation for emissions in selected UN regions*

2.5.3 Uncertainty Aggregation (Approach 1)

An easy method for combining uncertainties for a given model (e.g., calculating emissions from emissions factors and activity) is to propagate the sources of uncertainties by

$$\sigma_E = \sqrt{\sigma_A^2 + \sigma_B^2} \tag{24}$$

where σ_E is the uncertainty of the variable of interest, and σ_A^2 and σ_B^2 are the uncertainties of the sources. This is a practical and efficient method to combine uncertainties. We follow this approach to aggregate sources for emissions factors uncertainty and capacity factor.

2.5.4 Uncertainty Aggregation: Monte Carlo-based Uncertainty Quantification and Sensitivity Analysis (Approach 2)

Uncertainty quantification for activity and emissions was performed via Monte Carlo simulations. We followed the guidance provided in the IPCC. The Monte Carlo approach allows for a more flexible estimation of uncertainties and is more appropriate for propagating uncertainties when uncertainties can be large.

The first step was to identify the uncertainties and fitting probability density functions to the data if the underlying distribution is not known. It is important to consider possible correlations between uncertainty sources. Once the probability distributions were identified, iterations were started and random variables corresponding to each one of the uncertainty sources were drawn from their corresponding distributions. If correlations between the sources of uncertainty exist, then correlated variables are generated based on their correlation. For that task, we follow the copula method. Next, the variable of interest (e.g., emissions) is estimated from these random variables. This process was repeated over several iterations, forming a probability distribution function of the variable of interest. The mean of this distribution represents the final estimate. The uncertainty was then computed from the 95% empirical confidence interval by taking half of that confidence interval and dividing it by the mean. The resulting uncertainty was reported as percentage. The Monte Carlo simulations were repeated 10,000 times to generate the uncertainty distributions.

This approach was demonstrated at the country-level. Applying this to other GADM levels (e.g., GADM 2) would follow the same approach, with the exception of how the distributions were estimated. At the country-level, we used the aggregated values at all the available geographies for the country to fit a distribution for the variables of interest. At the GADM 2 level, these distributions could be constructed directly from the individual road segments. We found that at the country-level, over 80% of the countries contain sufficient geographies for estimating a

distribution. For countries without sufficient data to fit a distribution, it could be possible to leverage the distributions of nearby countries that might follow similar socio-economic patterns.

2.5.5 Capacity Uncertainty

Capacity was simply defined as the total length of the road network in an urban area. We used OpenStreetMap to estimate the capacity. There are many urban areas around the world for which OpenStreetMap data does not match the apparent road network. To estimate the possible overall road-network error, we used the work by Microsoft Bing Maps (Microsoft Bing Maps 2023). To estimate a standard deviation across the whole world, the missing road lengths were divided by the total road length for each set of areas that both values were available to create a list of fractions corresponding to the missing percentage. A standard deviation of 2% missing roads was then calculated from this set of data. To calculate the urban area level error, we assumed that:

$$\frac{\sigma_{CAP}}{CAP} = \sigma_l = 0.02 \tag{25}$$

Such that $\sigma_{CAP} = 0.02 \cdot CAP$ and we report σ_{CAP} for the capacity of each urban area source.

In later uncertainty calculations, we require an estimate of the per-road-segment capacity error. We simply assume that the 2% error is set appropriately to sum up to the correct error estimate. To do so, we set the per-segment standard deviation σ_{l_i} to:

$$\sigma_{l_i} = \frac{\sigma_l}{\sqrt{\sum_i l_i^2}} CAP \; l_i = \sigma_l' l_i \tag{26}$$

where l_i is the length of each road segment. This results in the same value for σ_{CAP} when calculated using propagation of errors for sums:

$$\sigma_{CAP} = \sqrt{\sum_i \sigma_{l_i}^2} = \sqrt{\sum_i (\sigma_l' l_i)^2} = \sqrt{\sigma_l'^2 \sum_i l_i^2} = \sigma_l' \cdot \sqrt{\sum_i l_i^2} = \frac{\sigma_l}{\sqrt{\sum_i l_i^2}} CAP \cdot \sqrt{\sum_i l_i^2}$$
$$= \sigma_l \cdot CAP \tag{27}$$

2.5.6 Activity Uncertainty

Uncertainties associated with activity are influenced directly by road segment length and AADT. While approaches for quantifying uncertainty in AADT exist, those primarily rely on available ground truth. Generalizing ground truth values from a specific region (e.g., USA) across the world will certainly introduce errors. Thus, activity uncertainty is estimated via Monte Carlo simulations by considering road segment length and AADT as the sources of uncertainty.

First, we observed that road segment length and AADT are often highly correlated. Therefore, it is necessary to ensure that the random variables generated in the Monte Carlo simulation are correlated as well. For this task, copulas are a great tool to generate correlated random variables drawn from a target distribution. The process of copulas starts by generating and fitting a copula (e.g., multivariate Gaussian) with similar correlations as the target data. Since the marginal

distributions are standard normal, it is possible to translate the marginals into uniform distributions and then generate samples from any of the target distributions.

Fitting distributions to road segment length and AADT, we observed that length follows either an exponential or beta distribution across all segment categories. The distribution of AADT varies and can be fit with log-normal and Weibull distributions.

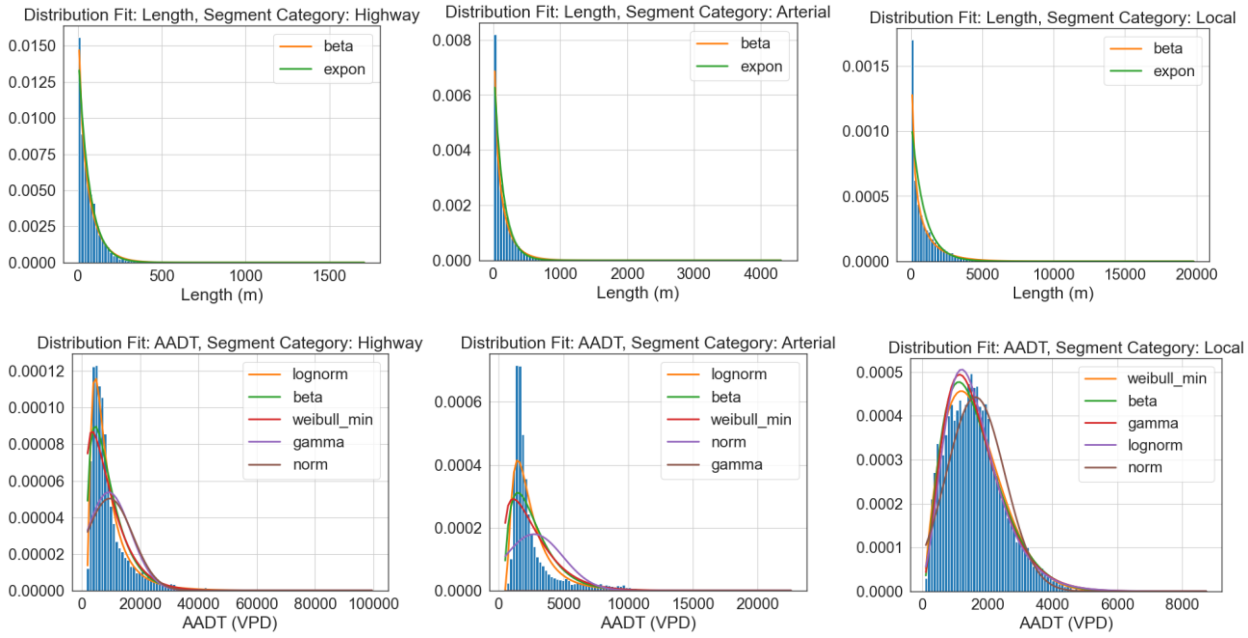

Figure 12 *Distribution fit for road segment length and AADT by segment category*

Activity uncertainty is then estimated via Monte Carlo simulations, for each segment category, for each country and month. The final uncertainty reported for each asset is aggregated over all segment category uncertainties following the uncertainty propagation method.

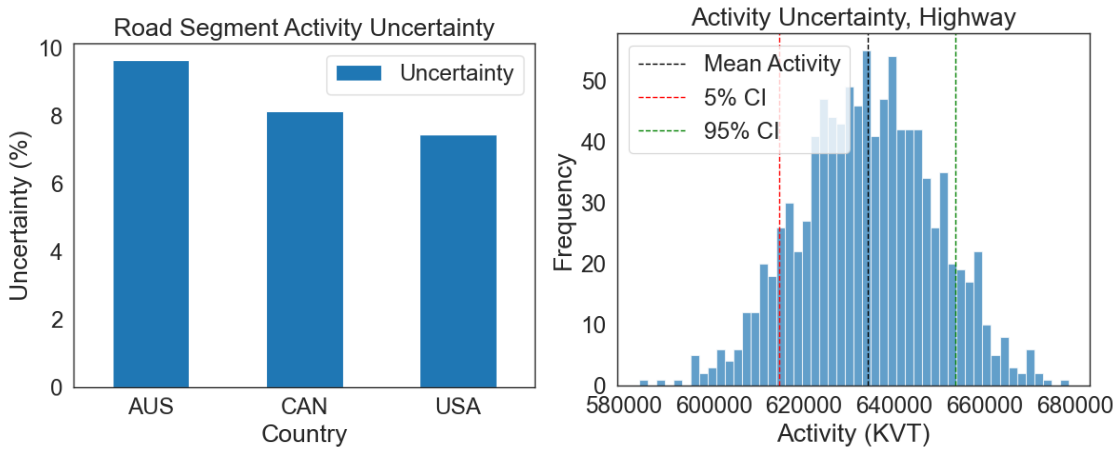

Figure 13 *Total propagated activity uncertainties by country and uncertainty confidence intervals from Monte Carlo simulations*

2.5.7 Emissions Uncertainty

To estimate uncertainties associated with estimates of emissions, we follow the IPCC guidance in the quantification of emissions' uncertainty. The sources of uncertainty are emissions factors and activity data. Following the Monte Carlo approach for uncertainty quantification, we fit distributions for emissions factors and activity. Based on our observations, activity and emissions factors can be treated as uncorrelated variables.

Distributions of CO_2 emissions factors data are estimated for each month at the country-level, for each segment category (local, arterial, highway). All geographies within a country contribute towards the distribution fit. We noted that the distributions within UN regions varied drastically, mostly driven by differences among countries. Therefore, in this section we focus on country-level uncertainties. Figure 14 shows the distribution fit for CO_2 emissions factors. In general, the distributions of CO_2 emissions factors have large outliers in their tails. Distributions for activity generally fit beta or exponential distributions.

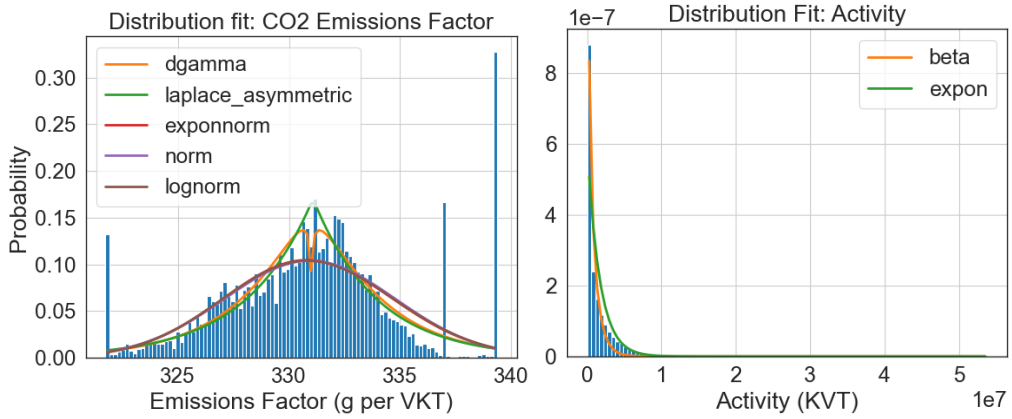

Figure 14 *Distribution fit for CO_2 emissions factor and activity*

It is expected that distributions of emissions factors will be largely influenced on the level of development of the country. On this dataset, only CO2 emissions factors vary monthly. Due to lack of data at higher temporal and spatial resolutions, all other emission factors are constant throughout the year and country. Understanding this limitation, we fit similar distributions of CO_2 (e.g., log-normal or normal) to other emissions factors.

Following the Monte Carlo approach, Figure 15 illustrates the resulting uncertainties for CO_2. We aggregate the uncertainties obtained for each segment category. Note that those are generally large already (~80%), so using the propagation method might not be the most appropriate.

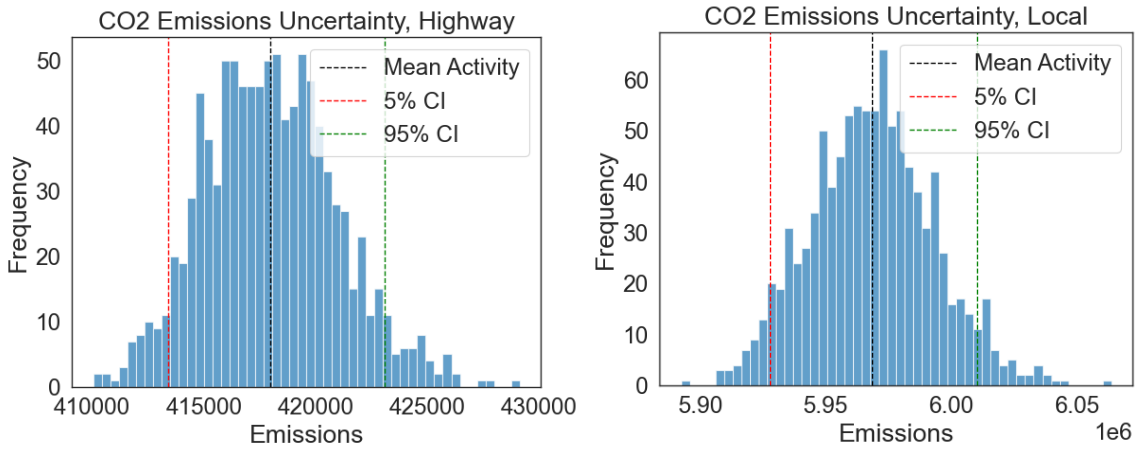

Figure 15 *CO_2 emissions uncertainty distributions for segment categories highway and local*

2.5.8 Emissions Factors Uncertainty

Sources for uncertainty in emissions factors depend on the gas. CO_2 emissions factors vary monthly and by geography, whereas the remaining emissions factors are constant for each year and country. We recognize that the lack of source data available at higher spatial and temporal resolutions contributes to systematic uncertainties and our results could include bias. To estimate emissions factors uncertainty, we follow the propagation of uncertainties by combining emissions and activity uncertainties.

2.5.9 Capacity Factor Uncertainty

Capacity factor uncertainty is computed following the propagation of capacity and activity uncertainties.

$$\sigma_{CF} = \sqrt{\left(\frac{ACT}{CAP}\right)^2 \left(\frac{\sigma_{CAP}^2}{CAP^2} + \frac{\sigma_{ACT}^2}{ACT^2}\right)} \tag{28}$$

where σ_{CAP}^2 is the capacity uncertainty and σ_{ACT}^2 is the activity uncertainty.

2.5.10 Total Equivalent CO_2: 20 and 100 Year Baselines

These two columns are calculated from propagation of error of the total:

$$TOT_Z = CO2 + CH4 \cdot CO2e_{CH4,Z} + N2O \cdot CO2e_{N2O,Z} \quad (29)$$

where $Z \in \{20,100\}$ are the two different baselines, $CO2e_{CH4,Z}$ is the equivalent CO_2 emissions for methane, and $CO2e_{N2O,Z}$ the equivalent CO_2 emissions for nitrous oxide. We use the propagation of error along with the standard IPCC definitions of error in the equivalent CO_2 emissions such that:

$$\sigma_{TOT_Z} = \sqrt{\sigma_{CO2}^2 + CH4^2\sigma_{CO2e_{CH4,Z}}^2 + CO2e_{CH4,Z}^2\sigma_{CH4}^2 + N2O^2\sigma_{CO2e_{N2OZ}}^2 + CO2e_{N2O,Z}^2\sigma_{N2O}^2} \quad (30)$$

2.5.11 Confidence

As described above, there are many assumptions and rough approximations made in order to estimate uncertainties of many different parameters calculated from our models. We judge, based on subject matter expertise and knowledge that this initial calculation is inadequate, that all uncertainty parameters calculated here have a LOW confidence using standard IPCC confidence ranges.

2.6 International Emissions Inventories

We have performed comparison against one international emissions inventory globally, EDGAR v8.0 (Crippa et al. 2020), for the years 2021-2022. Although we use EDGAR to get a global scale factor, this comparison is still valid to check the distribution of model performance and dependencies on input features. Specifically, the estimated global scale factor affects primarily the mean of our model output. EDGAR provides a global inventory for transportation that uses road density as a proxy to spatially distribute emissions. Other possible inventories, such as Google EIE or Carbon Monitor, for example, do not have open data sources that we could easily down load across our entire dataset. As a public, gridded product, the EDGAR dataset is somewhat more amenable to comparisons against our datasets.

Our emissions estimates were compared against EDGAR v8.0, both within the USA and globally. This comparison is performed for initial validation of our data; it is not used for uncertainty estimates. EDGAR v8.0 separates CO2 emissions by long-cycle (IEA-EDGAR CO2) and short-cycle (EDGAR CO2bio) sources; these are summed together for comparison to our data. EDGAR v8.0 also reports CO_2 emissions on a 0.1 degree grid, while we report our estimates on a 0.5 degree grid. To provide a consistent estimate across the two datasets, we aggregate the 0.1 grids to the nearest 0.5 grid and compare results on that.

See Section 3.3 for a discussion of the results of the comparison.

3 Results

In this section, we highlight top-level trends and differences between dataset release years. Specific information on per-urban-area emissions is available in the released dataset.

3.1 Machine Learning Model Ground Truth Comparison

While each trained ML model reduces the difference between the ground truth AADT values and the inferred values, it is worthwhile comparing a visual representation of the kinds of differences we see. Figures 16 and 17 below display a hexbin plot of predicted vs ground truth AADT values for the CNN Model, the GNN Model, and the ensemble for both the urban models (Figure 16) and the rural models (Figure 17).

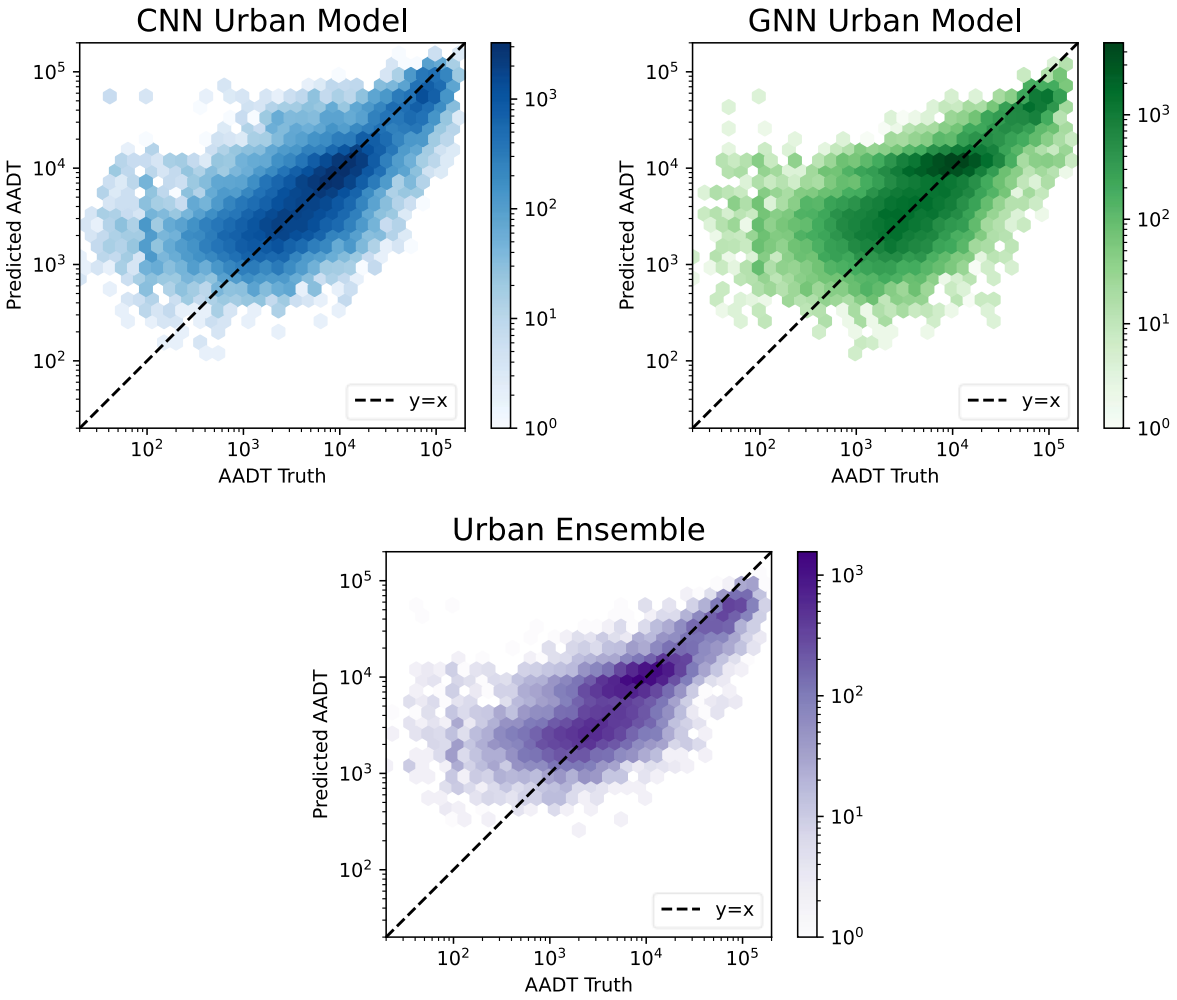

Figure 16 *Comparison of predicted AADT vs. ground truth across a set of 14 test cities in the USA for 2017 and 2018.*

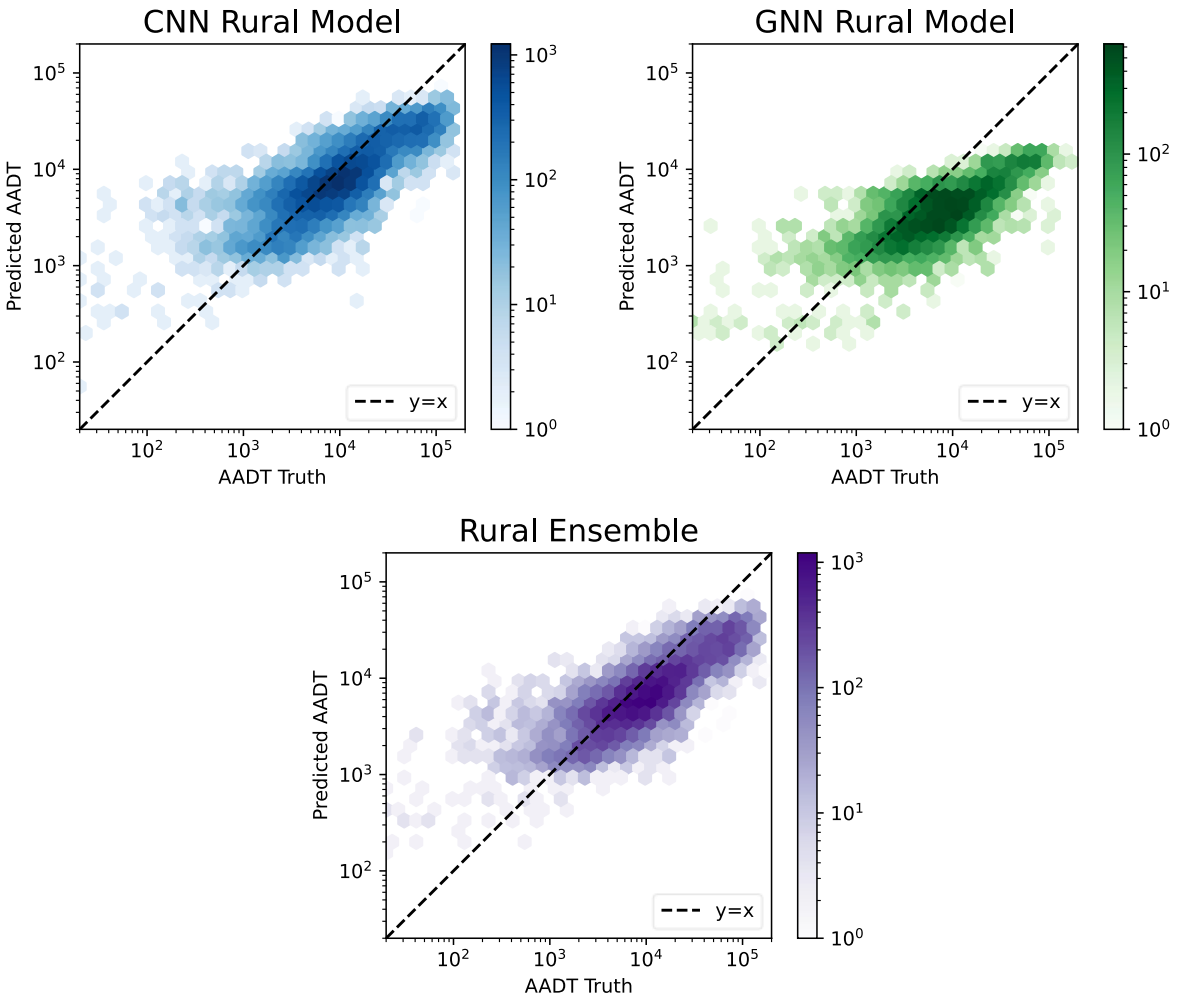

Figure 17 *Comparison of predicted AADT vs. ground truth across a set of 85 rural areas from 2017 and 77 rural areas from 2018 in the USA.*

The dashed lines in the plots indicate the line along with predicted and ground truth AADT values are equal. Bins within the plot that have a darker color are places which have more instances in that bin according to the color scale presented. We note in general, all models tend to overestimate AADT for low true AADT values, and models tend to slightly underestimate at the highest true AADT values. The underestimation at low AADT values is expected to be largely due to the bias in available truth AADT values towards more highly trafficked roads. Of special note, the GNN rural model more significantly underestimates true AADT values, though this is largely alleviated through ensembling with the CNN model.

3.2 Global Emissions Inventories Comparison

Figure 18 below shows the comparison between the EDGAR v8.0 dataset and our release of emissions estimates for the entire globe. EDGAR v8.0 emissions data is aggregated from a 0.1 degree grid to a 0.5 degree grid for comparison. We compare only for the years 2021-2022 and

aim to look at the dependencies of model performance on UN Region and on our rural/urban split. While there is a strong correlation across all emissions, there are also significant differences in areas with lower emissions. For example, where EDGAR broadly predicts 10^1 to 10^3 tons, our methodology predicts more. Where EDGAR broadly predicts 10^4 to 10^6 tons, our methodology also predicts less. For the purposes of this methodology document, we simply highlight that the two datasets provide comparable estimates when taken in aggregate.

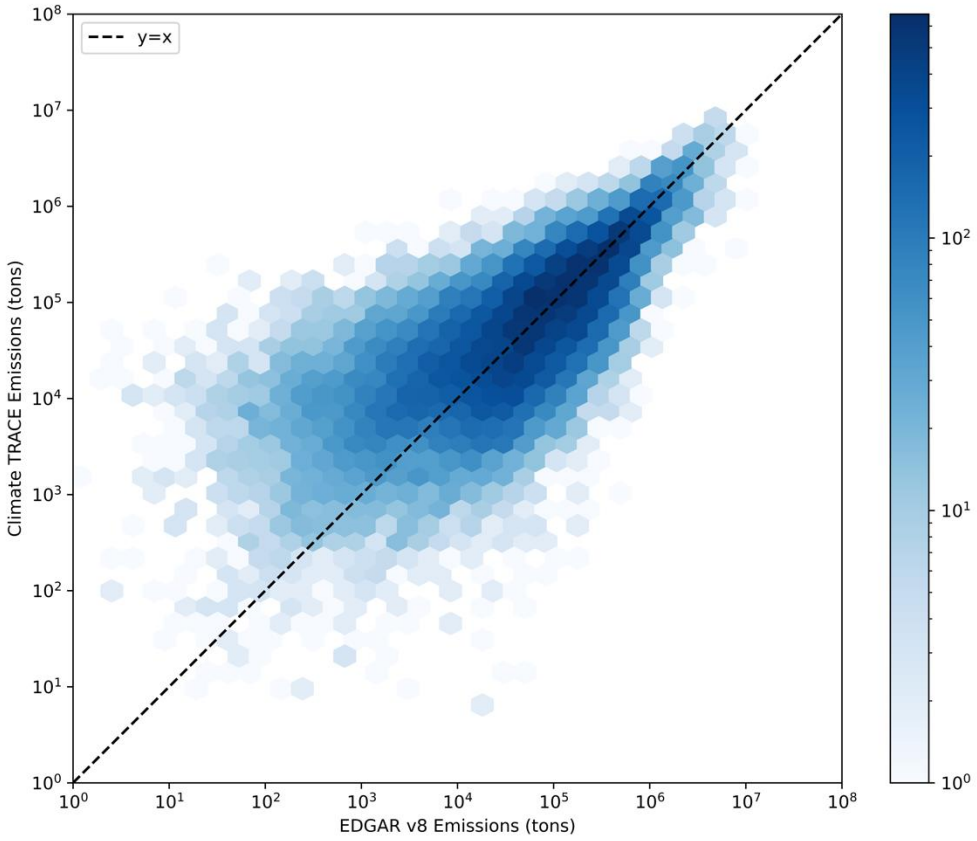

Figure 18 *Comparison of EDGAR v8.0 emissions and estimates described in this methodology across our global 0.5 degree grid. Darker blues indicate that the most common comparison between the two databases indicates that our methodology over-estimates emissions in lower values, and under-estimates larger values relative to EDGAR.*

Figure 18 shows our scaled emissions estimates compared with EDGAR v8.0 data. The global scale factor derived from EDGAR enforces that our estimates have a similar means, but we demonstrate that our emissions are similar in their dependency on other factors in the data as well. We further explore the discrepancies from EDGAR by determining whether the error is largely attributed to rural or urban areas. For each grid we calculate the fraction of the total urban area over the total area, with urban areas being defined using GHSL boundaries. Figure 19 shows the percent difference across various urban fraction bins.

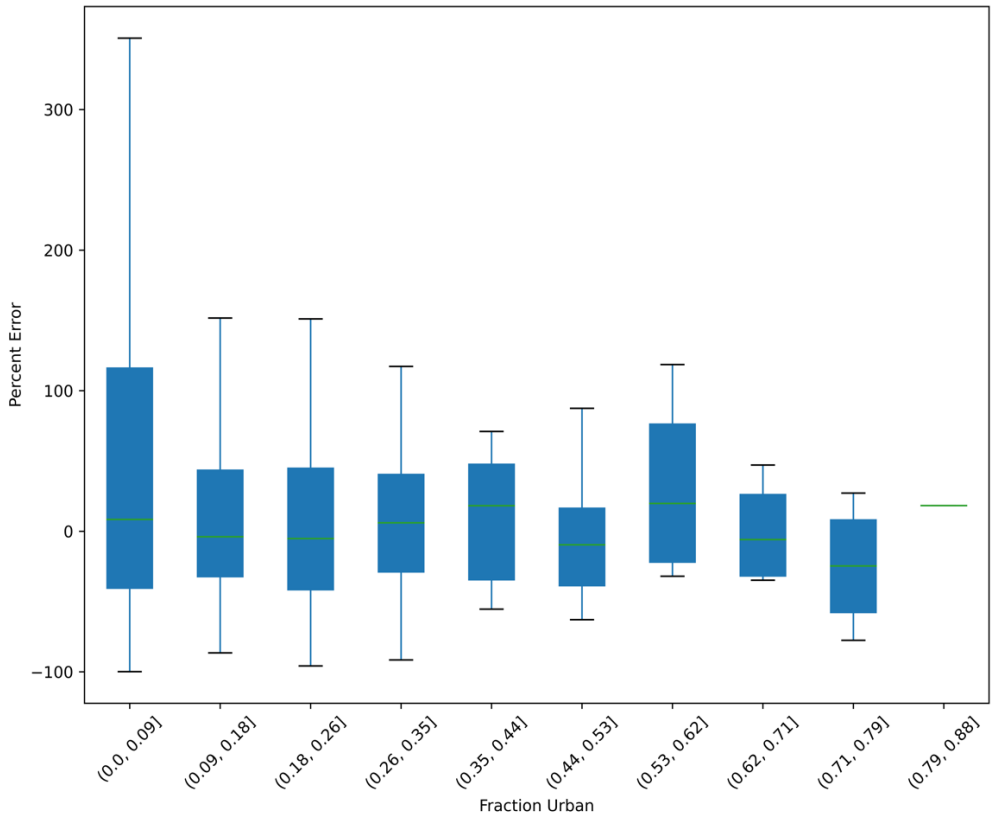

Figure 19 *Signed percent difference between EDGAR v8.0 and estimates across various urban fraction values.*

To further explore this difference in Figure 19, a Mann-Whitney U is performed between our error distributions for urban and rural areas. For this analysis, we choose grid points with urban fractions one standard deviation above the mean to be "urban", and all other points to be "rural". Figure 20 shows the result of this split. According to this threshold, rural areas contribute the most to our emissions. We sample 1000 points without replacement from both the distribution of the actual difference and percent difference between our model estimates and EDGAR. For the percent difference, there was no significant difference between urban ($\mu = 81.29$, $\sigma = 1076.1$) and rural ($\mu = 422.14$, $\sigma = 2486.9$) distributions with $u = 480861.0$, $p = 0.20$, *and* $Z = -1.48$. For the actual difference there was a significant difference between urban ($\mu = -35396.81$, $\sigma = 879676.63$) and rural ($\mu = -3629.71$, $\sigma = 119879.52$) distributions with $u = 525699.0$, $p = 0.03$, *and* $Z = 1.99$. This indicates that our model's relative performance between rural and urban areas is around the same, with the largest contribution to error being the magnitude of the emissions.

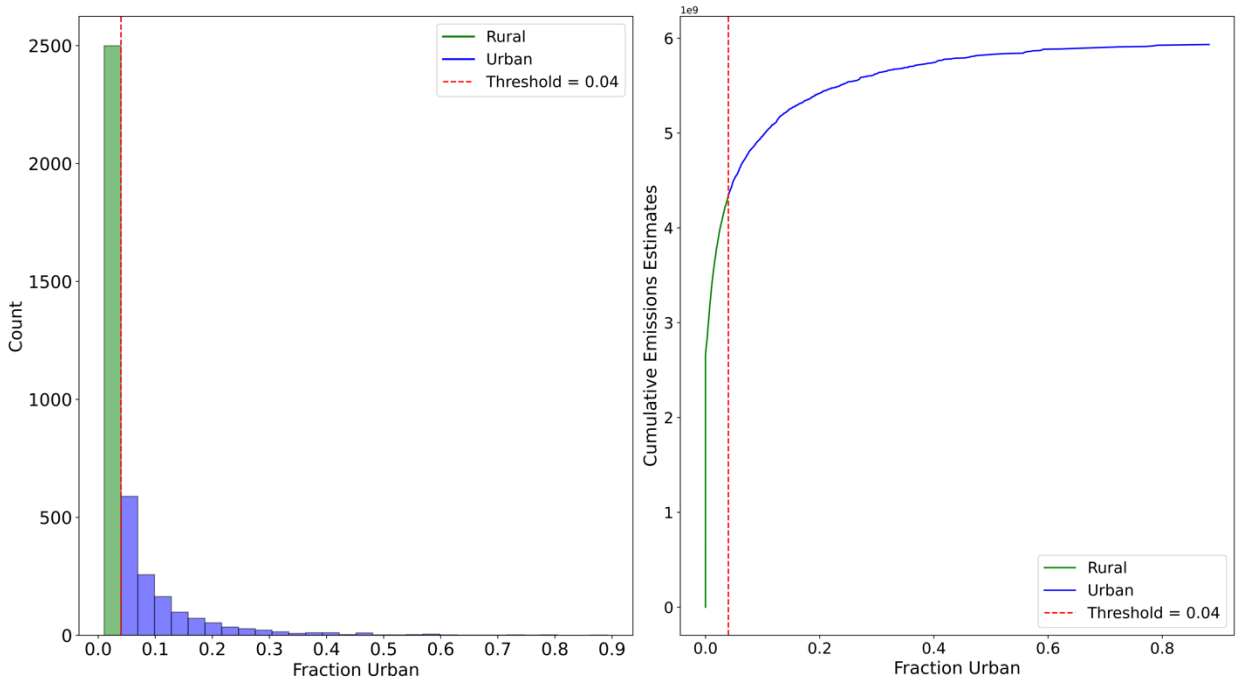

Figure 20 *Urban/rural split according to a 1-standard deviation above the mean for a given grid's fraction of urban atomic geometries.*

Lastly, we look at the difference between our estimates and EDGAR according to UN regions. Figure 21 below shows the absolute difference per each UN region, split up in rural and urban regions. The urban and rural regions are determined using the same method as above. For rural areas, our estimates differ the most in Eastern Asia, Southern Europe, and Western Europe. For urban areas, the largest difference is in Southern Asia and South-eastern Asia. Differences for all UN regions are provided in the appendix below (Figure 27).

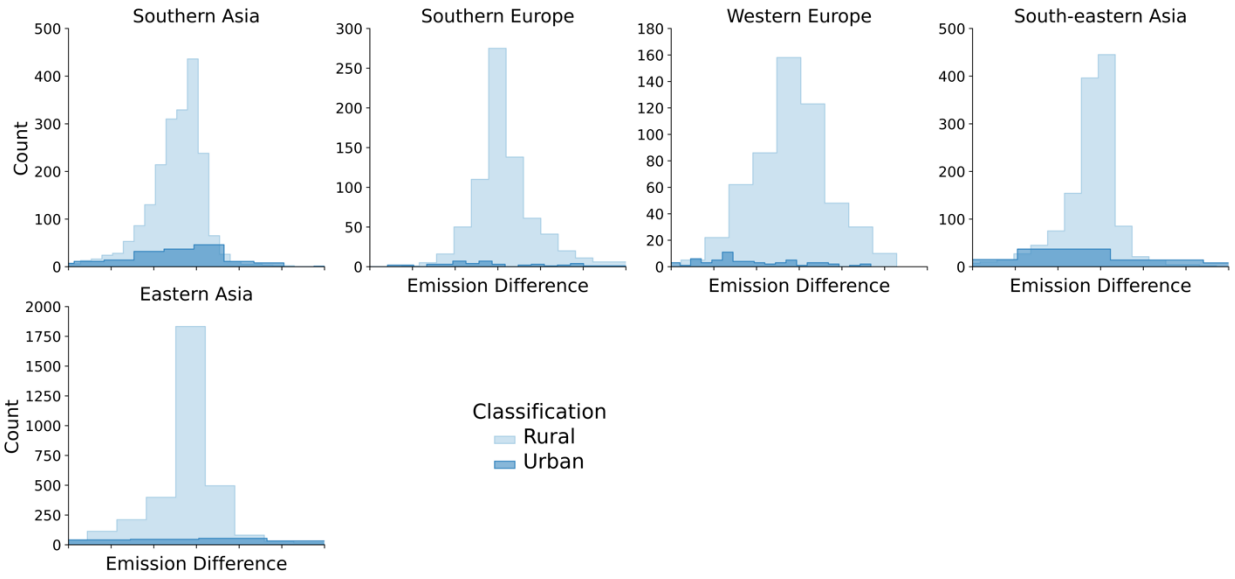

Figure 21 *Comparison of actual difference between estimates and EDGAR for key UN regions, split between rural and urban regions.*

Further international validation for both AADT and resulting emissions estimates is necessary, including a deeper understanding of all potential sources of differences (e.g., emissions factors uncertainty, varying total road network length included, etc.). We aim to incorporate more international AADT datasets, where available, into our model training and validation process. The addition of more real-time data (e.g., traffic and mobility) will help address the temporal ambiguity of our estimates. Finding publicly available data of this type remains a significant challenge.

3.3 Worldwide Emissions Results

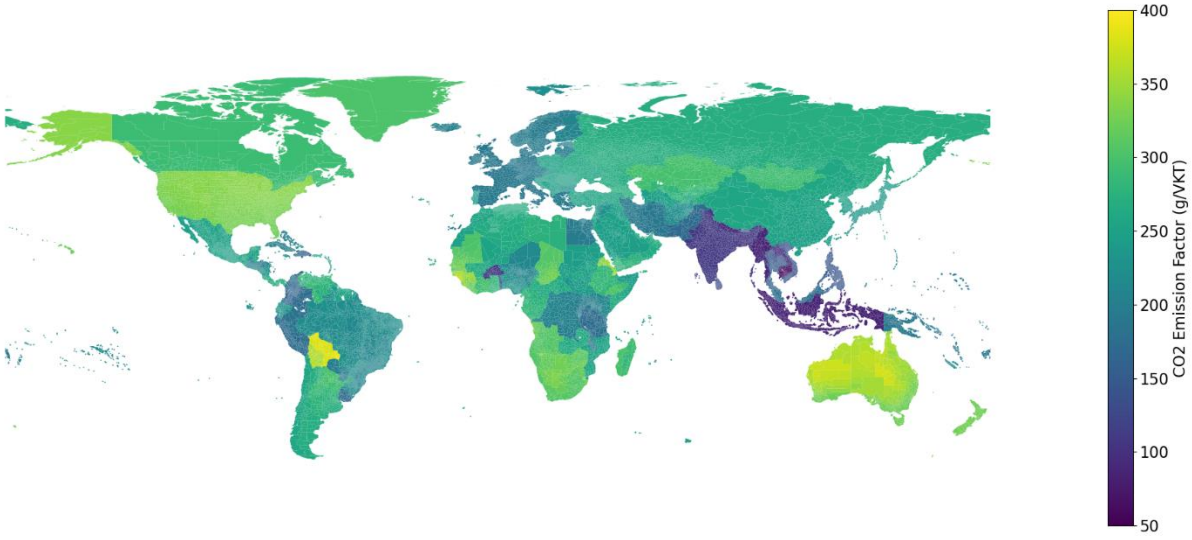

Figure 22 *Global map of the January 2023 emissions factor in the released data set. Units are grams per VKT. Regions shown are GADM Level-2 when available, GADM Level-1 otherwise.*

Figure 22 above shows an overview of the emissions factors for January, 2023 (EF, see Section 2.3.8). One interesting highlight from our data is the fact that areas in India and Indonesia have a much lower EF than countries such as China and the USA. This is mostly due to our data sources for vehicle fleet mix in those countries, which indicate that a vast majority of vehicles in those two countries are motorcycles. This is highlighted in Figure 23 below: Indonesia and India have vehicle registrations around 75% for motorcycles.

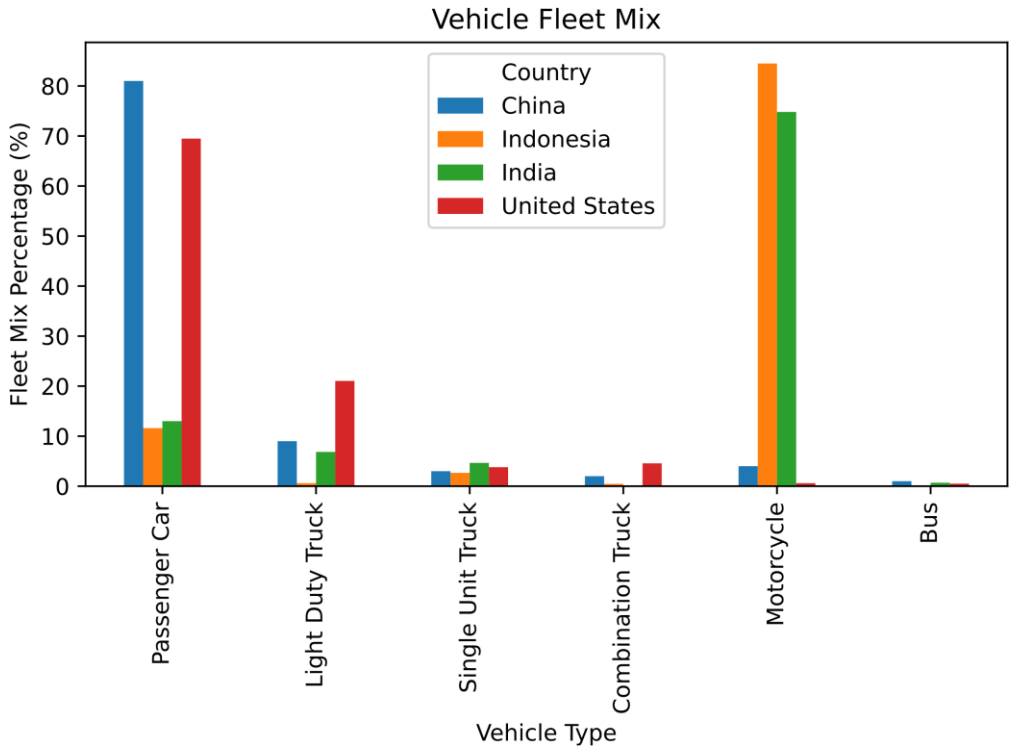

Figure 23 *Vehicle fleet mix for four countries highlighting the difference in motorcycle usage.*

In Figure 24, the effects of the temperature-based adjustments to fuel efficiency are shown (Section 2.2.9) by plotting the difference between the emission factors between July and January 2023. In locations such as the Southern U.S., there is a clear increase in the emission factor as January (winter) temperatures are close to the nominal 72° F and July (summer) temperatures are much higher than nominal. In locations such as Northern Australia, with summer in January, the reverse is true. More subtly, locations on the southern extremes of the southern continents show a higher emission factor in January than July; this is because the January temperatures are close to nominal (72° F) and the July temperatures are much colder (see Figure 8 for more details).

Additionally, Figure 25 displays the estimated total CO_2 emissions for 2023. Not unexpectedly, some of the highest emitting regions are in the U.S., Europe, and China. In contrast to Figure 22, the emissions in India and Indonesia are much more typical, as the comparatively low emission factors are balanced by higher activity.

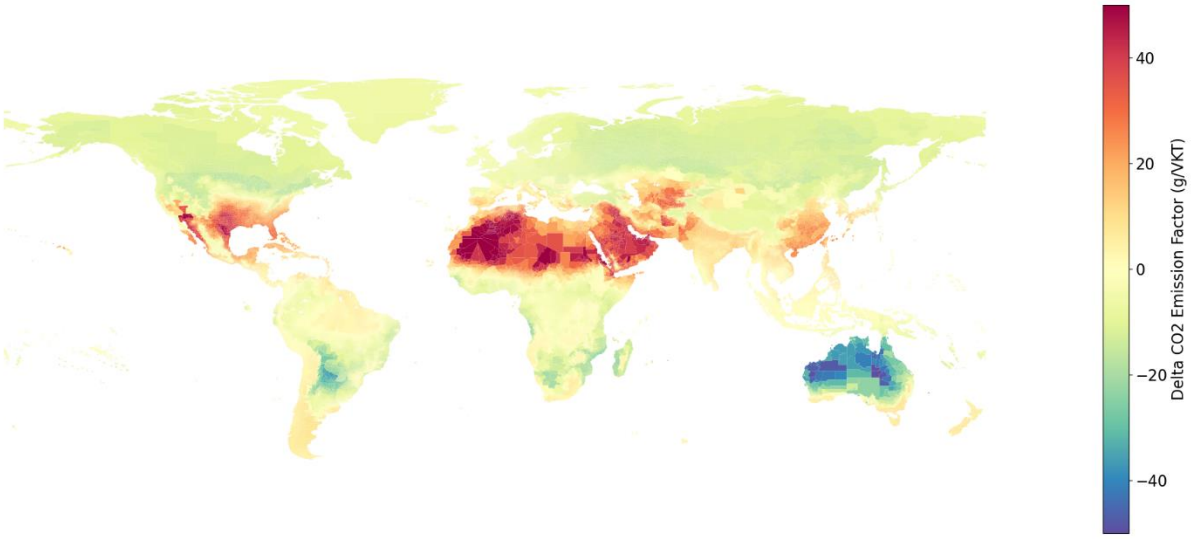

Figure 24 *Difference in CO_2 Emission Factor between July, 2023 and January, 2023. Units are grams per VKT. Regions shown are GADM Level-2 when available, GADM Level-1 otherwise.*

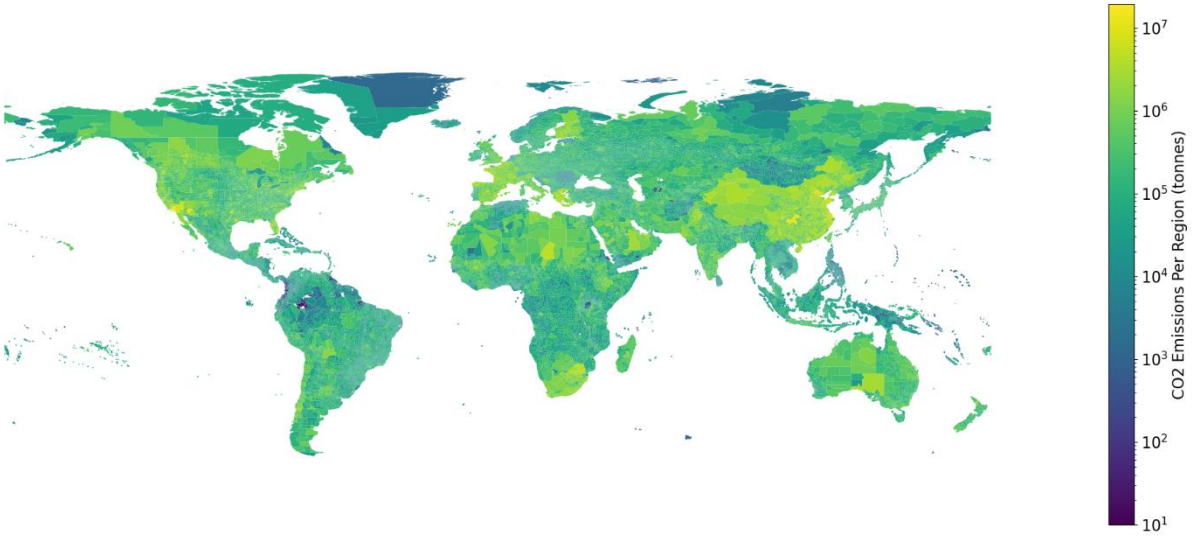

Figure 25 *Total estimated annual CO_2 emissions for 2023. Units are grams per VKT. Regions shown are GADM Level-2 when available, GADM Level-1 otherwise. Note emissions are shown per region; locations where an area is broken into many small GADM Level-2 regions will show much lower emissions than an equivalently emitting location of the same area contained within just one GADM Level-2 region.*

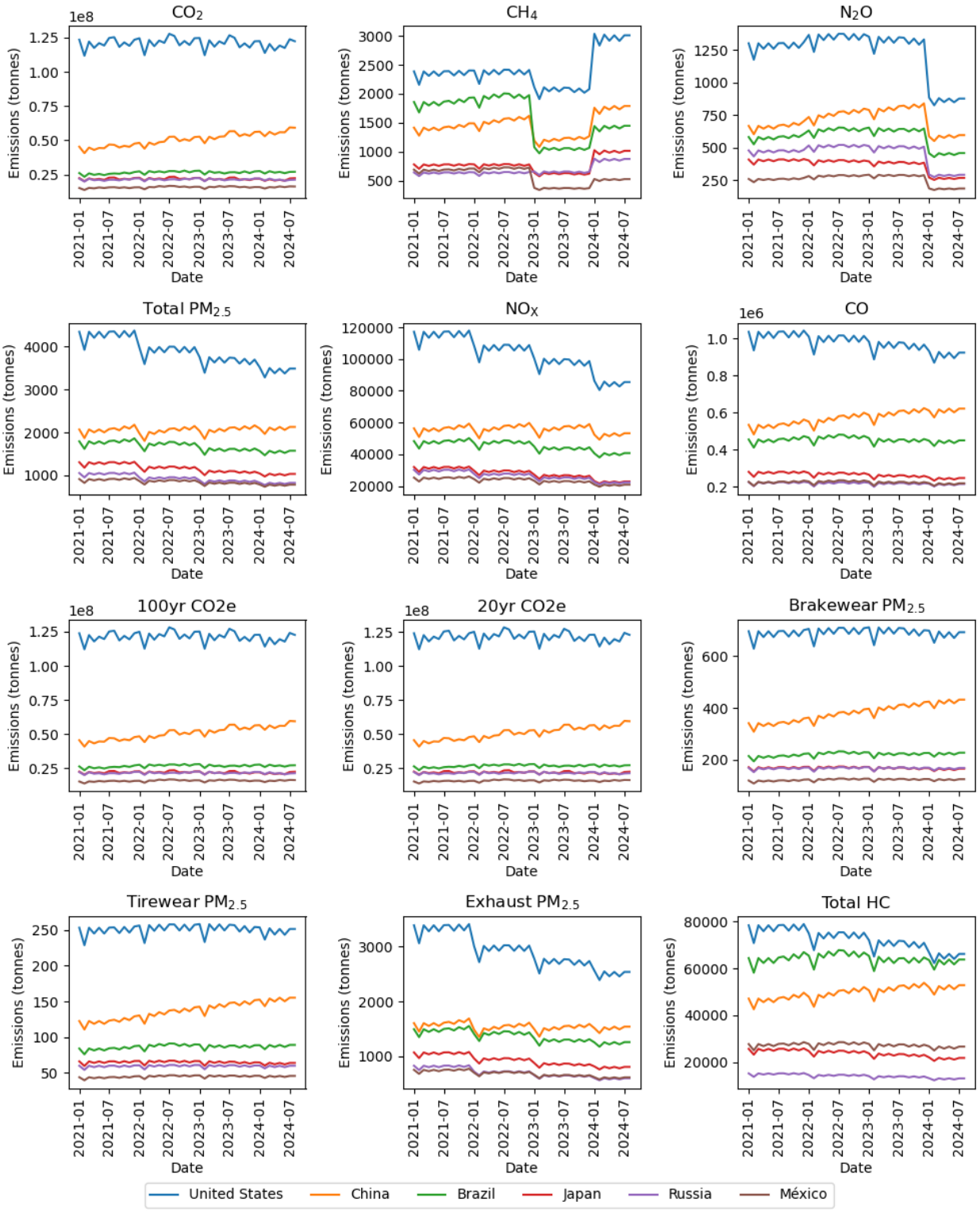

Figure 26 *Monthly emissions for the top 6 emitting countries (by 100yr CO2e in 2023) for all estimated gases*

Figure 26 shows the estimated emissions on a monthly basis for six of the top emitting countries for all twelve of the modeled GHG and non-GHG emissions. In these plots, for some of the emissions other than CO_2, such as CH_4 and N_2O, there are apparent step changes in emissions at annual boundaries; this traces to changes in emission factors derived from EPA data which is provided on annual intervals (Section 2.2.10). A future implementation will smooth these changes by linearly interpolating the emission factors.

Additional highlights include:

- We estimate that between 2022 and 2023, an extra 73×10^6 extra tonnes of CO_2 were emitted from road transportation; this is a 1.1% increase
- Per country income class, between 2022 and 2023 we estimate HIC[1] saw a decrease of 9×10^6 tonnes of CO_2, while UMIC increased by 40×10^6 tonnes, LMIC by 32×10^6 tonnes, and LIC by 11×10^6 tonnes
- Of the 2023 estimated emissions, 52% is from HIC, 32% UMIC, 12% LMIC, and 4% LIC

4 Conclusions

We have presented a hybrid road transportation emissions estimation method that is detailed, scalable, and easy to update. The ability to calculate emissions per road segment can be further refined to reach an unprecedented level of detail and global coverage. Where available, the integration of real-time traffic data would increase the temporal resolution and accuracy of our models. This type of actionable emissions monitoring data will be critical to ensuring we meet global emissions reduction targets and may inspire new ways of mitigating the effects of climate change. Finally, more local vehicle registration or usage data would improve our emissions estimates regardless of a change in the underlying model predictions of average traffic.

We have also developed an uncertainty quantification pipeline (see Section 2.5) that integrates IPCC's Approach 1 (propagation of uncertainty) and Approach 2 (Monte Carlo simulations) for combining uncertainties. Various areas for further exploration remain, including improving aspects of the data and the uncertainty quantification process. One opportunity for reducing uncertainty is to improve the spatial and temporal resolution of the variables contributing to emission factors, and extending emissions factors by vehicle years. In extending uncertainty analyses, we will continue exploring the uncertainties of urban and rural regions separately. We noted that the distribution of emissions factors varied by urban and region areas, with rural emissions factors often dominating the overall distribution of emissions factors and separate treatment of those distributions may be beneficial. Sensitivity analyses to identify the contributions to uncertainty of each variable will be helpful, as well as assessing uncertainty in trends.

[1] HIC: High income country, UMIC: Upper-middle income country, LMIC: Lower-middle income country, LIC: Low-income country, as defined by the World Bank: https://datahelpdesk.worldbank.org/knowledgebase/articles/906519.

5 Acknowledgements

Thanks to Aaron Davitt and Lekha Sridhar from WattTime for their help in reviewing our methodology. We thank previous APL ASPIRE Intern Kevin Zhang for their work in helping extend the vehicle fleet database to many additional countries.

6 Supplementary Materials

6.1 Vehicle Fleet Mix Sources

Table 8 *List of Vehicle Fleet Mix Sources for specific countries*

Reference: ACEA dataset: (ACEA - European Automobile Manufacturers' Association 2022).	
• Russian Federation • Republic of Turkiye • United Kingdom of Great Britain and Northern Ireland • Federal Republic of Germany • French Republic • Kingdom of Spain • Italian Republic • Republic of Poland	• Kingdom of the Netherlands • Portuguese Republic • Kingdom of Belgium • Kingdom of Sweden • Czech Republic • Kingdom of Denmark • Ireland • Republic of Finland
Reference: UNECE dataset: (UNECE - United Nations Economic Commission for Europe 2022)	
● Hellenic Republic ● Republic of Belarus ● State of Israel ● Republic of Azerbaijan ● Swiss Confederation ● Republic of Hungary ● Republic of Austria ● Republic of Bulgaria ● Republic of Croatia ● Republic of Albania ● Republic of Lithuania	● Republic of Moldova ● Bosnia and Herzegovina ● Republic of Latvia ● Republic of Cyprus ● Republic of Estonia ● Republic of Slovenia ● Republic of Malta ● Republic of Iceland ● Grand Duchy of Luxembourg ● Montenegro
Reference: WHO dataset (World Health Organization 2018)	
• Republic of Indonesia • Japan • Arab Republic of Egypt • Islamic Republic of Iran • Republic of the Philippines • Republic of Colombia • Republic of Iraq	• Republic of Benin • State of Palestine • Lebanese Republic • Togolese Republic • Republic of Paraguay • State of Libya • Republic of Honduras • Republic of El Salvador

• Kingdom of Thailand • Bolivarian Republic of Venezuela • Republic of the Sudan • Kingdom of Morocco • Republic of Peru • Republic of Ghana • Commonwealth of Australia • United Republic of Tanzania • Islamic Republic of Afghanistan • Republic of Ecuador • Republic of Cote d'Ivoire • Republic of Senegal • Syrian Arab Republic • Republic of Kazakhstan • United Arab Emirates • Democratic Socialist Republic of Sri Lanka • Dominican Republic • Romania • Plurinational State of Bolivia • Federal Democratic Republic of Nepal • Republic of Tunisia • Burkina Faso • Republic of Cuba • Republic of Guinea • Republic of Zimbabwe	• Kingdom of Cambodia • Republic of Madagascar • Republic of Costa Rica • Republic of Burundi • Republic of Panama • Oriental Republic of Uruguay • Republic of South Sudan • State of Eritrea • Republic of Liberia • Sultanate of Oman • Republic of Rwanda • Mongolia • Kingdom of Norway • Republic of the Gambia • Slovak Republic • Republic of Botswana • Lao People's Democratic Republic • Republic of Trinidad and Tobago • Republic of Mauritius • Republic of Namibia • Democratic Republic of Timor-Leste • Co-operative Republic of Guyana • Republic of Suriname • Republic of Maldives • Barbados • Belize

- Other Countries for which we have specific data:
    - Argentina (ARG): (ADEFA n.d.)
    - Australia (AUS): ("Motor Vehicle Census, Australia, 31 Jan 2021 | Australian Bureau of Statistics" 2021)
    - Brazil (BRA): ("Fleet Size of the Auto Industry in Brazil by Type 2021" 2022)
    - Canada (CAN); (Government of Canada 2020)
    - Chile (CHL) https://www.ine.cl/docs/default-source/parque-...
    - People's Republic of China (CHN)
    - Guatemala (GTM)
    - India (IND): Road Transport Yearbook
    - Indonesia (IDN)
    - Japan (JPN)
    - Kuwait (KWT)
    - Malaysia (MYS)
    - Myanmar (MMR)

- Singapore (SGP)

6.2 Supplementary materials metadata

***Table** S1 General dataset information*

General Description	Definition
Sector definition	Emissions from all road-based transportation such as cars, buses, motorcycles, and trucks.
UNFCCC sector equivalent	1.A.3.b ("Road Transportation")
Temporal Coverage	2015 – 2024
Temporal Resolution	Monthly
Data format(s)	CSV
Coordinate Reference System	EPSG:4326, decimal degrees
Number of sources available for download and percent of global emissions (as of 2024)	Almost 48,000 GADM Level-2 regions covering the entire globe with the exception of Antarctica
Total emissions for 2023	6.51×10^9 tonnes of 100yr CO2e
Ownership	N/A: estimates rely on modeling individual vehicles; no ownership is possible.
What emission factors were used?	Model based
What is the difference between a "NULL / none / nan" versus "0" data field?	"0" values are for true non-existent emissions. If we know that the sector has emissions for that specific gas, but the gas was not modeled, this is represented by "NULL/none/nan"
total_CO2e_100yrGWP and total_CO2e_20yrGWP conversions	Climate TRACE uses IPCC AR6 CO2e GWPs. CO_2e conversion guidelines are here: https://www.ipcc.ch/report/ar6/wg1/downloads/report/IPCC_AR6_WGI_FullReport_small.pdf

***Table S2** Asset level metadata description*

Data attribute	Definition
sector	Transportation
asset_sub-sector_name	Road transportation

Data attribute	Definition
asset definition	Emissions from on-road transportation by GADM based administrative regions. See Section 2.2.2.
start_date	Start date for time period of emissions estimation (YYYY-MM-DD format)
end_date	End date for time period of emissions estimation (YYYY-MM-DD format)
asset_identifier	GADM Level-1 or GADM Level-2 GADM ID
model_number	String identifying model & source data version
asset_name	GADM Level-1 or GADM Level-2 name
iso3_country	ISO 3166-1 alpha-3 country code for city taken from GADM ADM_2 layer value
location	GADM Level-1 or GADM Level-2 GADM ID
type	Not used; N/A
capacity_description	Total road network length for each region. See Section 2.3.4
capacity_units	kilometers
capacity_factor_description	Monthly activity divided by capacity for each region. See Section 2.3.8
capacity_factor_units	vehicles per month
activity_description	Total vehicle kilometers traveled (VKT) per month for each region. See Section 2.3.5
activity_units	vehicle-kilometers per month
CO2_emissions_factor	tonnes CO_2/VKT; see Section 2.3.8
CH4_emissions_factor	tonnes CH_4/VKT; see Section 2.3.8
N2O_emissions_factor	tonnes N_2O/VKT; see Section 2.3.8
PM2_5_emissions_factor	tonnes Total $PM_{2.5}$/VKT; see Section 2.3.8

Data attribute	Definition
NOX_emissions_factor	tonnes Total NO_X/VKT; see Section 2.3.8
CO_emissions_factor	tonnes Total CO/VKT; see Section 2.3.8
CO2_emissions	tonnes CO_2; see Section 2.3.1
CH4_emissions	tonnes CH_4; see Section 2.3.1
N2O_emissions	tonnes N_2O; see Section 2.3.1
PM2_5_emissions	tonnes Total $PM_{2.5}$; see Section 2.3.1
NOX_emissions	tonnes NO_x; see Section 2.3.1
CO_emissions	tonnes CO; see Section 2.3.1
total_CO2e_100yrGWP	tonnes 100yr CO_2e; see Section 2.3.1
total_CO2e_20yrGWP	tonnes CO_2e; see Section 2.3.1
other1_description	The GADM ID of the parent region; for GADM Level-2 assets, this is the GADM Level-1 ID; for GADM Level-1 assets, this is the GADM Level-0 ID
other1_units	N/A
other2_description	The GADM ID of the asset
other2_units	N/A
other3_description	The GADM level of the asset
other3_units	N/A
other4_description	$PM_{2.5}$ emissions from brakewear
other4_units	tonnes
other5_description	$PM_{2.5}$ emissions from tirewear
other5_units	tonnes
other6_description	$PM_{2.5}$ emissions from exhaust

Data attribute	Definition
other6_units	tonnes
other7_description	Total non-GHG HC emissions
other7_units	tonnes
other8_description	N/A
other8_units	N/A
other9_description	N/A
other9_units	N/A
other10_description	N/A
other10_units	N/A

Table S3 *Asset level metadata description confidence and uncertainty*

Data attribute	Confidence Definition	Uncertainty Definition
type	Not used; N/A	Not used; N/A
capacity_description	See Section 3.2.7	See Section 3.2.2
capacity_units	See Section 3.2.7	Kilometers
capacity_factor_description	See Section 3.2.7	N/A
capacity_factor_units	See Section 3.2.7	N/A
activity_description	See Section 3.2.7	See Section 3.2.3
activity_units	See Section 3.2.7	vehicle-kilometers
CO2_emissions_factor	See Section 3.2.7	See Section 3.2.5
CH4_emissions_factor	See Section 3.2.7	See Section 3.2.5
N2O_emissions_factor	See Section 3.2.7	See Section 3.2.5

Data attribute	Confidence Definition	Uncertainty Definition
other_gas_emissions_factor	See Section 3.2.7	N/A
CO2_emissions	See Section 3.2.7	See Section 3.2.4
CH4_emissions	See Section 3.2.7	See Section 3.2.4
N2O_emissions	See Section 3.2.7	See Section 3.2.4
other_gas_emissions	See Section 3.2.7	N/A
total_CO2e_100yrGWP	See Section 3.2.7	See Section 3.2.6
total_CO2e_20yrGWP	See Section 3.2.7	See Section 3.2.6

6.3 Coefficient of Variation; Additional Plots

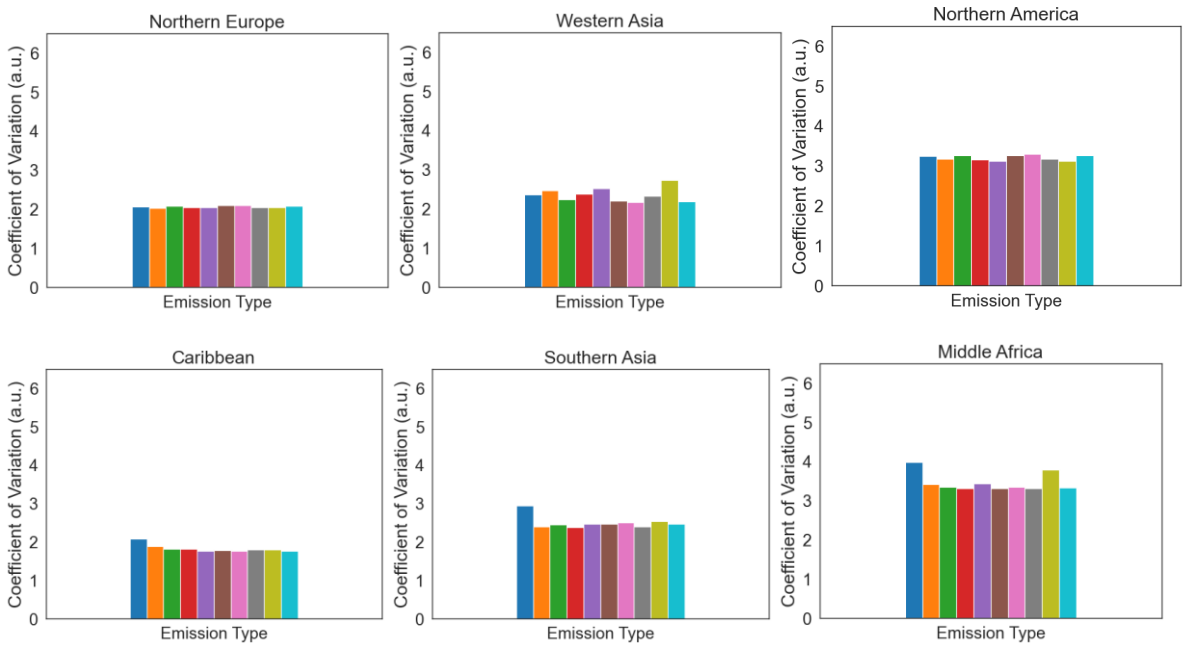

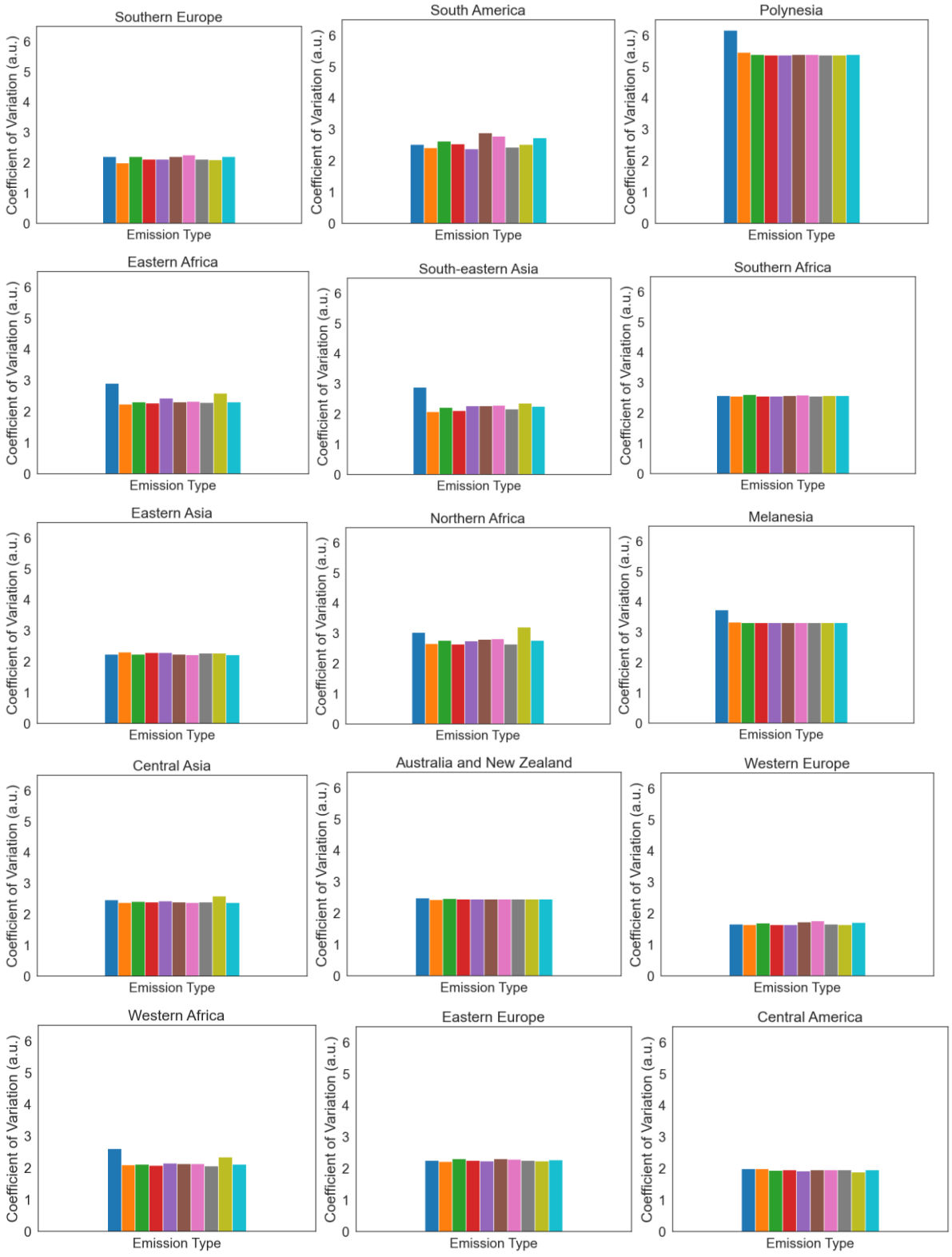
Southern Europe
South America
Polynesia
Eastern Africa
South-eastern Asia
Southern Africa
Eastern Asia
Northern Africa
Melanesia
Central Asia
Australia and New Zealand
Western Europe
Western Africa
Eastern Europe
Central America
Coefficient of Variation (a.u.)
Emission Type
0
1
2
3
4
5
6

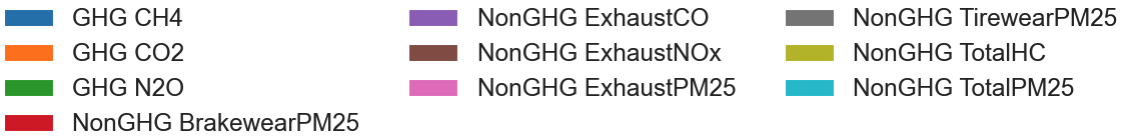

Figure 27 *Coefficient of variation for emissions in each UN region*

6.4 Difference between estimates and EDGAR

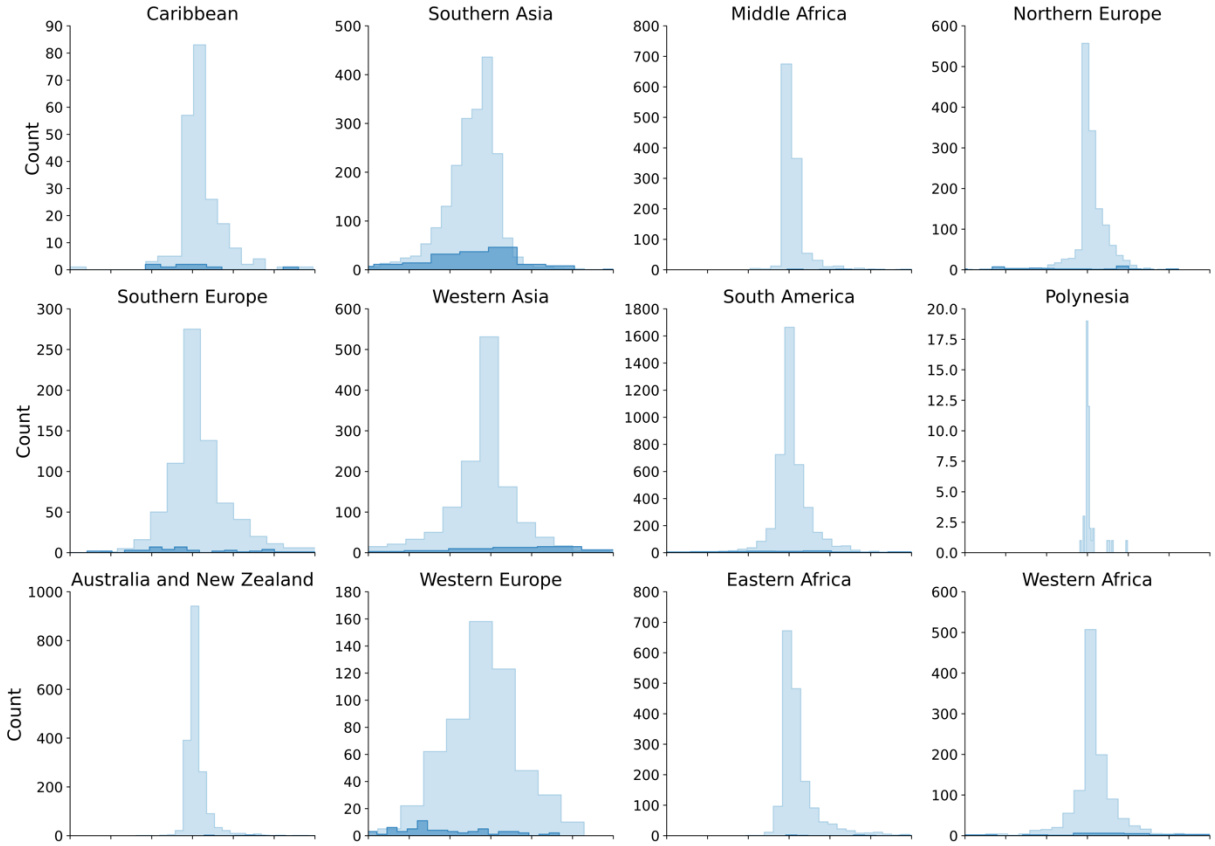

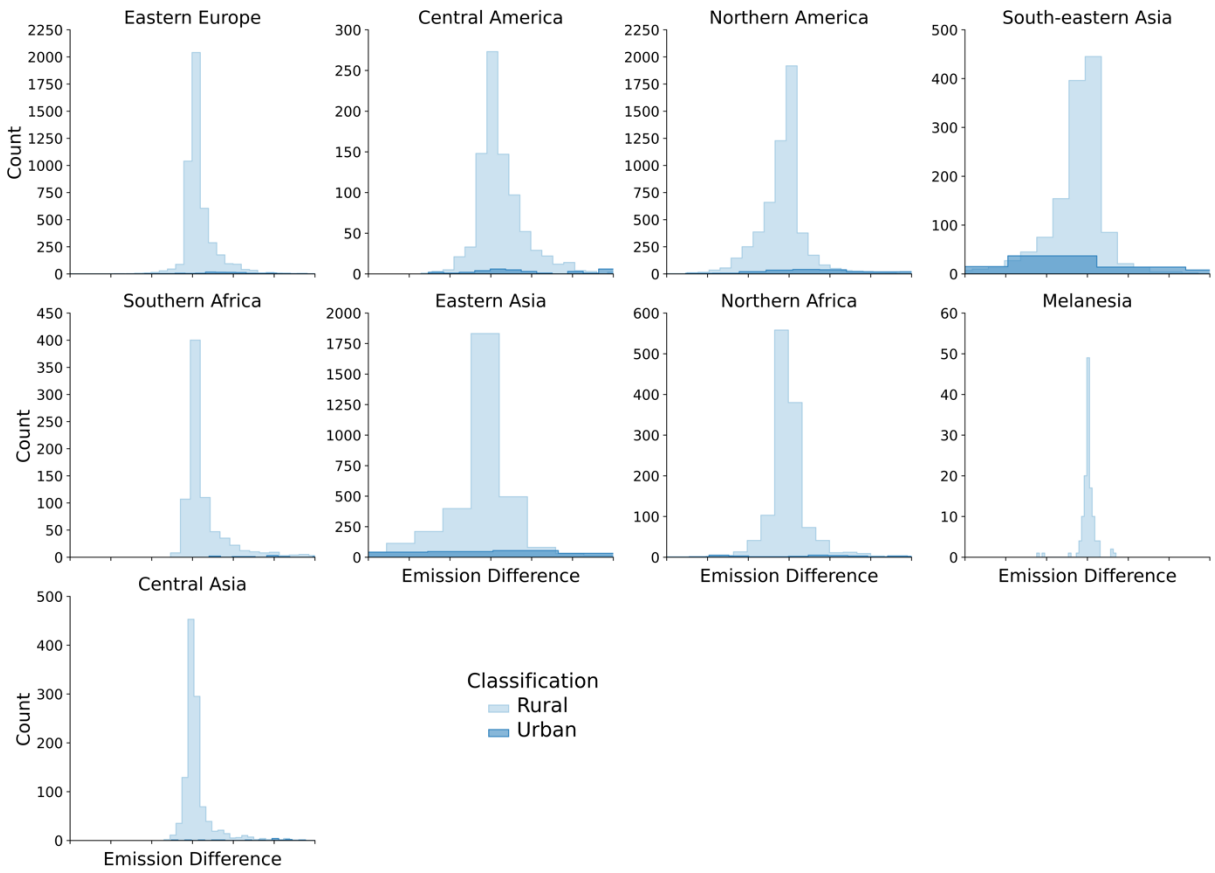

Figure 27 Comparison of actual difference between estimates and EDGAR for all UN regions, split between rural and urban regions.

7. Administrative Concerns

7.1. Permissions and Use

All Climate TRACE data is freely available under the Creative Commons Attribution 4.0 International Public License, unless otherwise noted below.

7.2. Citation format

Tomek M. Kott, Kevin Foster, Marisel Villafane-Delgado, Wayne Loschen, Patrick Sicurello, Melat Ghebreselassie, Elizabeth Reilly, and Marisa Hughes (2024). *Transportation Sector: Global Road Emissions*. The Johns Hopkins University Applied Physics Laboratory (JHU/APL), Laurel, MD, USA, Climate TRACE Emissions Inventory. https://climatetrace.org [Accessed date]

7.3. Geographic boundaries and names (iso3_country data attribute):

The depiction and use of boundaries, geographic names and related data shown on maps and included in lists, tables, documents, and databases on Climate TRACE are generated from the Global Administrative Areas (GADM) project (Version 4.1 released on 16 July 2022) along with their corresponding ISO3 codes, and with the following adaptations:

- HKG (China, Hong Kong Special Administrative Region) and MAC (China, Macao Special Administrative Region) are reported at GADM level 0 (country/national);
- Kosovo has been assigned the ISO3 code 'XKX';
- XCA (Caspian Sea) has been removed from GADM level 0 and the area assigned to countries based on the extent of their territorial waters;
- XAD (Akrotiri and Dhekelia), XCL (Clipperton Island), XPI (Paracel Islands) and XSP (Spratly Islands) are not included in the Climate TRACE dataset;
- ZNC name changed to 'Turkish Republic of Northern Cyprus' at GADM level 0;
- The borders between India, Pakistan and China have been assigned to these countries based on GADM codes Z01 to Z09.

The above usage is not warranted to be error free and does not imply the expression of any opinion whatsoever on the part of Climate TRACE Coalition and its partners concerning the legal status of any country, area or territory or of its authorities, or concerning the delimitation of its borders.

7.4. Disclaimer

The emissions provided for this sector are our current best estimates of emissions, and we are committed to continually increasing the accuracy of the models on all levels. Please review our terms of use and the sector-specific methodology documentation before using the data. If you identify an error or would like to participate in our data validation process, please contact us.

8. References

1. ACEA - European Automobile Manufacturers' Association. 2022. "Report - Vehicles in Use, Europe 2022." https://www.acea.auto/publication/report-vehicles-in-use-europe-2022/.
2. ADEFA. n.d. "Anuario 2020 | Estadísticas." ADEFA. Accessed December 14, 2022. http://adefa.org.ar/es/estadisticas-anuarios-interno?id=55.
3. Boeing, Geoff. 2017. "OSMnx: New Methods for Acquiring, Constructing, Analyzing, and Visualizing Complex Street Networks." *Computers, Environment and Urban Systems* 65 (September): 126–39. https://doi.org/10.1016/j.compenvurbsys.2017.05.004.
4. Brody, S., U. Alon, & E. Yahav. 2022. "How Attentive are Graph Attention Networks?" *International Conference on Learning Representations*. https://openreview.net/forum?id=F72ximsx7C1
5. Bronstein, Michael M., Joan Bruna, Yann LeCun, Arthur Szlam, and Pierre Vandergheynst. 2017. "Geometric Deep Learning: Going beyond Euclidean Data." *IEEE Signal Processing Magazine* 34 (4): 18–42. https://doi.org/10.1109/MSP.2017.2693418.
6. Crippa, Monica, Efisio Solazzo, Ganlin Huang, Diego Guizzardi, Ernest Koffi, Marilena Muntean, Christian Schieberle, Rainer Friedrich, and Greet Janssens-Maenhout. 2020. "High Resolution Temporal Profiles in the Emissions Database for Global Atmospheric Research." *Scientific Data* 7 (1): 1–17. https://doi.org/10.1038/s41597-020-0462-2.
7. Drusch, Matthias, Umberto Del Bello, Sébastien Carlier, Olivier Colin, Veronica Fernandez, Ferran Gascon, Bianca Hoersch, et al. 2012. "Sentinel-2: ESA's Optical High-Resolution Mission for GMES Operational Services." *Remote Sensing of Environment*.
8. Fan, Tongle, Guanglei Wang, Yan Li, and Hongrui Wang. 2020. "MA-Net: A Multi-Scale Attention Network for Liver and Tumor Segmentation." *IEEE Access*.

9. "Fleet Size of the Auto Industry in Brazil by Type 2021." 2022. *Statista*. https://www.statista.com/statistics/787327/automobile-industry-fleet-size-brazil-vehicle-type/.
10. Florczyk, A., C. Corbane, M. Schiavina, M. Pesaresi, L. Maffenini, M. Melchiorri, P. Politis, et al. 2019. "GHS Urban Centre Database 2015, Multitemporal and Multidimensional Attributes, R2019A." European Commission, Joint Research Centre (JRC). https://data.jrc.ec.europa.eu/dataset/53473144-b88c-44bc-b4a3-4583ed1f547e.
11. Gately, Conor K, L.R. Hutyra, and I.S. Wing. 2019. "DARTE Annual On-Road CO2 Emissions on a 1-Km Grid, Conterminous USA V2, 1980-2017." ORNL Distributed Active Archive Center. https://doi.org/10.3334/ORNLDAAC/1735.
12. Gately, Conor K, Lucy R Hutyra, and Ian Sue Wing. 2015. "Cities, Traffic, and CO_2: A Multidecadal Assessment of Trends, Drivers, and Scaling Relationships." *Proceedings of the National Academy of Sciences*.
13. Global Administrative Areas. 2022. "GADM Database of Global Administrative Areas, Version 4.1." https://www.gadm.org.
14. Government of Canada, Statistics Canada. 2020. "Vehicle Registrations, by Type of Vehicle, Inactive." September 10, 2020. https://www150.statcan.gc.ca/t1/tbl1/en/tv.action?pid=2310006701.
15. Gurney, Kevin R, Jianming Liang, Risa Patarasuk, Yang Song, Jianhua Huang, and Geoffrey Roest. 2020. "The Vulcan Version 3.0 High-Resolution Fossil Fuel CO_2 Emissions for the United States." *Journal of Geophysical Research: Atmospheres*.
16. Harris, I., T. J. Osborn, P. Jones, and D. Lister. 2020. "Version 4 of the CRU TS monthly high-resolution gridded multivariate climate dataset." *Scientific Data*, 7(1). https://doi.org/10.1038/s41597-020-0453-3
17. International Energy Agency. 2019. "Transport Sector CO2 Emissions by Mode in the Sustainable Development Scenario, 2000-2030 – Charts – Data & Statistics." IEA. March 27, 2019. https://www.iea.org/data-and-statistics/charts/transport-sector-co2-emissions-by-mode-in-the-sustainable-development-scenario-2000-2030.
18. Jochen Topf. 2023. "Osmium: Command Line Tool for Working with OpenStreetMap Data Based on the Osmium Library." https://osmcode.org/osmium-tool/.
19. Liu, Zhu, Philippe Ciais, Zhu Deng, Steven Davis, Bo Zheng, Yilong Wang, Duo Cui, et al. 2020. "Carbon Monitor, a near-Real-Time Daily Dataset of Global CO2 Emission from Fossil Fuel and Cement Production." *Scientific Data* 7 (November). https://doi.org/10.1038/s41597-020-00708-7.
20. Lohse-Busch, H., M. Duoba, E. Rask, K. Stutenberg, V. Gowri, L. Slezak, and D. Anderson. 2013. "Ambient Temperature (20°F, 72°F and 95°F) Impact on Fuel and Energy Consumption for Several Conventional Vehicles, Hybrid and Plug-In Hybrid Electric Vehicles and Battery Electric Vehicle". *SAE Technical Paper Series*. https://doi.org/10.4271/2013-01-1462
21. Main-Knorn, M., B. Pflug, J. Louis, V. Debaecker, U. Müller-Wilm, and F. Gascon. 2017. "Sen2Cor for Sentinel-2." In *Image and Signal Processing for Remote Sensing XXIII*, 10427:37–48. IEEE.
22. Microsoft Bing Maps. 2023. "Road Detections." Microsoft. https://github.com/microsoft/RoadDetections.

23. "Motor Vehicle Census, Australia, 31 Jan 2021 | Australian Bureau of Statistics." 2021. June 30, 2021. https://www.abs.gov.au/statistics/industry/tourism-and-transport/motor-vehicle-census-australia/latest-release.
24. Mukherjee, Ryan, Derek Rollend, Gordon Christie, Armin Hadzic, Sally Matson, Anshu Saksena, and Marisa Hughes. 2021. "Towards Indirect Top-Down Road Transport Emissions Estimation." In *2021 IEEE/CVF Conference on Computer Vision and Pattern Recognition Workshops (CVPRW)*, 1092–1101. https://doi.org/10.1109/CVPRW53098.2021.00120.
25. OpenStreetMap Contributors. 2020. "OpenStreetMap: User-Generated Street Maps." https://planet.osm.org.
26. Scheibenreif, Linus M., Michael Mommert, and Damian Borth. 2021. "Estimation of Air Pollution with Remote Sensing Data: Revealing Greenhouse Gas Emissions from Space." In *ICML 2021 Workshop on Tackling Climate Change with Machine Learning*. https://www.climatechange.ai/papers/icml2021/23.
27. UNECE - United Nations Economic Commission for Europe. 2022. "Road Vehicle Fleet at 31 December by Fuel Type, Type of Vehicle,Country and Year." https://w3.unece.org/PXWeb2015PXWeb2015/pxweb/en/STAT/STAT__40-TRTRANS__03-TRRoadFleet/03_en_TRRoadFuelFlt_r.px/.
28. US EPA. 2022. "GHG Emissions Factors Hub." https://www.epa.gov/system/files/documents/2022-04/ghg_emission_factors_hub.pdf.
29. ———. 2023. "Inventory of U.S. Greenhouse Gas Emissions and Sinks: 1990-2021." https://www.epa.gov/ghgemissions/inventory-us-greenhouse-gas-emissions-and-sinks-1990-2021.
30. US FHWA. 2017. "Highway Performance Monitoring System (HPMS) Data." https://www.fhwa.dot.gov/policyinformation/hpms.
31. ———. 2018. "State Motor-Vehicle Registrations." https://www.fhwa.dot.gov/policyinformation/statistics/2018/mv1.cfm.
32. ———. 2020. "Distribution of Annual Vehicle Distance Traveled - Percentage by Vehicle Type Rural/Urban (Table VM-4)." https://www.fhwa.dot.gov/policyinformation/statistics/2020/vm4.cfm.
33. World Bank Group. 2019. "CURB: Climate Action for Urban Sustainability, Version 2.1." https://datacatalog.worldbank.org/search/dataset/0042029.
34. World Health Organization. 2018. *Global Status Report on Road Safety 2018*. Genève, Switzerland: World Health Organization. https://www.who.int/publications-detail-redirect/9789241565684.
35. World Resources Institute. 2022. "Greenhouse Gas (GHG) Emissions | Climate Watch." 2022. https://www.climatewatchdata.org/ghg-emissions.